

Understanding the nature of luminous red galaxies (LRGs): Connecting LRGs to central and satellite subhalos

Shogo Masaki^{1,2,*†}, Chiaki Hikage³, Masahiro Takada⁴, David N. Spergel^{4,5},
and Naoshi Sugiyama^{1,3,4}

¹ Department of Physics, Graduate School of Science, Nagoya University, Aichi 464-8602, Japan

² NTT Secure Platform Laboratories, Tokyo 180-8585, Japan

³ Kobayashi Maskawa Institute (KMI), Nagoya University, Aichi 464-8602, Japan

⁴ Kavli Institute for the Physics and Mathematics of the Universe (Kavli IPMU, WPI), The University of Tokyo, Chiba 277-8582, Japan

⁵ Department of Astrophysical Sciences, Princeton University, Peyton Hall, Princeton NJ 08544, USA

18 October 2018

ABSTRACT

We develop a novel abundance matching method to construct a mock catalog of luminous red galaxies (LRGs) in the Sloan Digital Sky Survey (SDSS), using catalogs of halos and subhalos in N -body simulations for a Λ -dominated, cold dark matter model. Motivated by observations suggesting that LRGs are passively-evolving, massive early-type galaxies with a typical age $\gtrsim 5$ Gyr, we assume that simulated halos at $z = 2$ ($z2$ -halo) are progenitors for LRG-host subhalos observed today, and we label the most tightly bound particles in each progenitor $z2$ -halo as LRG “stars”. We then identify the subhalos containing these stars to $z = 0.3$ (SDSS redshift) in descending order of the masses of $z2$ -halos until the comoving number density of the matched subhalos becomes comparable to the measured number density of SDSS LRGs, $\bar{n}_{\text{LRG}} = 10^{-4} h^3 \text{ Mpc}^{-3}$. Once the above prescription is determined, our only free parameter is the number density of halos identified at $z = 2$ and this parameter is fixed to match the observed number density at $z = 0.3$. By tracing subsequent merging and assembly histories of each progenitor $z2$ -halo, we can directly compute, from the mock catalog, the distributions of central and satellite LRGs and their internal motions in each host halo at $z = 0.3$. While the SDSS LRGs are galaxies selected by the magnitude and color cuts from the SDSS images and are not necessarily a stellar-mass-selected sample, our mock catalog reproduces a host of SDSS measurements: the halo occupation distribution for central and satellite LRGs, the projected auto-correlation function of LRGs, the cross-correlation of LRGs with shapes of background galaxies (LRG-galaxy weak lensing), and the nonlinear redshift-space distortion effect, the Finger-of-God effect, in the angle-averaged redshift-space power spectrum. The mock catalog generated based on our method can be used for removing or calibrating systematic errors in the cosmological interpretation of LRG clustering measurements as well as for understanding the nature of LRGs such as their formation and assembly histories.

Key words: cosmology: theory – galaxy clustering – galaxy formation – cosmology: large-scale structure of the Universe

1 INTRODUCTION

Galaxy redshift surveys are one of the primary tools for studying the large-scale structure in the Universe (Davis & Huchra 1982; de Lapparent et al. 1986; Kirshner et al. 1987; York et al. 2000; Peacock et al. 2001). Over the coming decade, astronomers will have even larger surveys including BOSS¹ (Dawson et al. 2013),

WiggleZ² (Blake et al. 2011), VIPERS³, FMOS⁴, HETDEX⁵, Big-BOSS⁶ (Schlegel et al. 2009), Subaru Prime Focus Spectrograph

* E-mail: shogo.masaki@nagoya-u.jp

† JSPS Fellow

¹ <http://cosmology.lbl.gov/BOSS/>

² <http://wigglez.swin.edu.au/site/>

³ <http://vipers.inaf.it/>

⁴ <http://www.naoj.org/Observing/Instruments/FMOS/>

⁵ <http://hetdex.org/>

⁶ <http://bigboss.lbl.gov/>

(PFS⁷; Ellis et al. 2012), Euclid⁸, and WFIRST⁹. The upcoming generation of galaxy redshift surveys is aimed at understanding cosmic acceleration as well as measuring the composition of the Universe via measurements of both the geometry and the dynamics of structure formation (Wang et al. 1999; Eisenstein et al. 1999; Tegmark et al. 2004; Cole et al. 2005).

On large scales, galaxies trace the underlying distribution of dark matter, and their clustering correlation is a standard tool to extract cosmological information from the measurement. Because of their relatively high spatial densities and their intrinsic bright luminosities, luminous red galaxies (LRGs) are one of the most useful tracers (Eisenstein et al. 2001; Wake et al. 2006). Measurements of the clustering properties of LRGs have been used to measure the baryon acoustic oscillation (BAO) scale (Eisenstein et al. 2005; Percival et al. 2007; Anderson et al. 2012) as well as to constrain cosmological parameters (Tegmark et al. 2004; Cole et al. 2005; Reid et al. 2010; Saito et al. 2011).

Our lack of a detailed understanding of the relationship between galaxies and their host halos complicates the analysis of large-scale clustering data. The halo occupation distribution (HOD) approach or the halo model approach has provided a useful, albeit empirical, approach to relating galaxies to dark matter (see e.g., Peacock & Smith 2000; Seljak 2000; Scoccimarro et al. 2001, for the pioneer works). In these approaches, the distribution of halos is first modeled for a given cosmological model, e.g. by using N -body simulations, and then galaxies of interest are populated into dark matter halos. The previous works have shown that, by adjusting the model parameters, the HOD based model well reproduces the auto-correlation functions of LRGs measured from the Sloan Digital Sky Survey¹⁰ (SDSS) (Zehavi et al. 2005; Zheng et al. 2007; Wake et al. 2008; Reid & Spergel 2009; White et al. 2011). It has been shown that LRGs reside in massive halos with a typical mass of a few times $10^{13} h^{-1} M_{\odot}$. However, the HOD method employs several simplified assumptions. For instance, the distribution of galaxies is assumed to follow that of dark matter in their host halo and the model assumes a simple functional form for the HOD.

An alternative approach is the so-called abundance matching method. The abundance matching method directly connects target galaxies to simulated subhalos assuming a tight and physically-motivated relation between their properties, e.g., galaxy luminosity and subhalo circular velocity, without employing any free fitting parameters (e.g., Kravtsov et al. 2004; Conroy et al. 2006; Trujillo-Gomez et al. 2011; Reddick et al. 2012; Masaki et al. 2013; Nuza et al. 2012). However, it is not still clear whether the method can simultaneously reproduce different clustering measurements such as the auto-correlation function and the galaxy-galaxy weak lensing (Neistein & Khochfar 2012). Most of the previous studies use only the auto-correlation function to test their abundance matching model.

In this paper, we develop an alternative approach to the abundance matching method for constructing a mock catalog of LRGs. Motivated by observations suggesting that LRGs are passive, massive early-type galaxies, which are believed to have formed at $z > 1$ (Masjedi et al. 2008; Carson & Nichol 2010; Tojeiro et al. 2012), we assume that the progenitor halos for LRG-host subhalos are formed at $z = 2$. We identify massive halos at this redshift, de-

fine the innermost particles of each progenitor halo as hypothetical “LRG-star” particles, follow the star particles to lower redshifts, and then identify subhalos at $z = 0.3$ containing these star particles. We adjust the number of halos identified as LRG progenitors at $z = 2$ to match the observed number density of the SDSS LRGs, $\bar{n}_{\text{LRG}} \simeq 10^{-4} h^3 \text{ Mpc}^{-3}$ (also see Conroy et al. 2008; Seo et al. 2008, for a similar-idea based approach when connecting galaxies to halos). With this method, we can directly trace, from the simulations, how each progenitor halo at $z = 2$ experiences merger(s), is destroyed or survives at lower redshift as well as which progenitor halos become central or satellite subhalos (galaxies) in each host halo at $z = 0.3$. Thus, our method allows us to include assembly/merging histories of the LRG-progenitor halos. Our method is solely based on a mass-selected sample of progenitor halos at $z = 2$ and does not have *any* free fitting parameter because the mass threshold is fixed by matching to the number density of SDSS LRGs. We compare statistical quantities computed from our mock catalog with the SDSS measurements: the HOD, the projected auto-correlation function of LRGs, the LRG-galaxy weak lensing and the redshift-space power spectrum of LRGs. Even though our method is rather simple, we show that our mock catalog remarkably well reproduces the different measurements simultaneously.

The structure of this paper is as follows. In Section 2, we describe our method to generate a mock catalog of LRGs by using N -body simulations for a Λ -dominated cold dark matter (Λ CDM) model as well as the catalogs of halos and subhalos at $z = 2$ and $z = 0.3$. In Section 3, we show the model predictions on the relation between LRGs and dark matter, and compare with the SDSS measurements. Section 4 is devoted to discussion and conclusion.

2 METHODS

2.1 Cosmological N -body simulations

Throughout this paper we use two realizations of cosmological N -body simulations generated using the publicly-available *Gadget-2* code (Springel et al. 2001b; Springel 2005). For each run, we employ a flat Λ CDM cosmology with $\Omega_m = 0.272$, $\Omega_b = 0.0441$, $\Omega_{\Lambda} = 0.728$, $H_0 = 100h = 70.2 \text{ km s}^{-1} \text{ Mpc}^{-1}$, $\sigma_8 = 0.807$ and $n_s = 0.961$ using the same parameters and notation as in the the *WMAP* 7-yr analysis (Komatsu et al. 2011). Our simulation of larger-size box, which we hereafter call “L1000”, employs 1024^3 dark matter particles in a box of $1 h^{-1} \text{ Gpc}$ on a side. The L1000 simulation allows for a higher statistical precision in measuring the correlation functions from the mock catalog. To test the effect of numerical resolution on our results, we also use a higher resolution simulation that employs 1024^3 particles in a box of $300 h^{-1} \text{ Mpc}$. We call the smaller-box simulation “L300”. The mass resolution for the simulations (mass of an N -body particle) is $7 \times 10^{10} h^{-1} M_{\odot}$ or $1.9 \times 10^9 h^{-1} M_{\odot}$ for L1000 or L300, respectively. The initial conditions for both the simulation runs are generated using the second-order Lagrangian perturbation theory (Crocce et al. 2006; Nishimichi et al. 2009) and an initial matter power spectrum at $z = 65$, computed from the *CAMB* code (Lewis et al. 2000). We set the gravitational softening parameter to be 30 and $8 h^{-1} \text{ kpc}$ for the L1000 and L300 runs, respectively.

We use the friends-of-friends (FoF) group finder (e.g., Davis et al. 1985) with a linking length of 0.2 in units of the mean interparticle spacing to create a catalog of halos from the simulation output and use the *SubFind* algorithm (Springel et al. 2001a)

⁷ <http://sumire.ipmu.jp/pfs/intro.html>

⁸ <http://sci.esa.int/euclid>

⁹ <http://wfirst.gsfc.nasa.gov/>

¹⁰ <http://www.sdss.org/>

to identify subhalos within each halo. In this paper, we use halos and subhalos that contain more than 20 particles. Each particle in a halo region is assigned to either a smooth component of the parent halo or to a satellite subhalo, where the smooth component contains the majority of N -body particles in the halo region. Hereafter we call the smooth component a central subhalo and call the subhalo(s) satellite subhalo(s). For each subhalo, we estimate its mass by counting the bounded particles, which we call the subhalo mass (M_{sub}). We store the position and velocity data of particles in halos and subhalos at different redshifts. To estimate the virial mass (M_{vir}) for each parent halo, we apply the spherical overdensity method to the FoF halo, where the spherical boundary region is determined by the interior virial overdensity, Δ_{vir} , relative to the mean mass density (Bryan & Norman 1998). The overdensity $\Delta_{\text{vir}} \simeq 268$ at $z = 0.3$ for the assumed cosmological model. The virial radius is estimated from the estimated mass as $R_{\text{vir}} = (3M_{\text{vir}}/4\pi\bar{\rho}_{m0}\Delta_{\text{vir}})^{1/3}$, where $\bar{\rho}_{m0}$ is the comoving matter density.

2.2 Mock catalog of LRGs: connecting halos at $z = 2$ to central and satellite subhalos at $z = 0.3$

LRGs are very useful tracers of large-scale structure as they can reach a higher redshift, thereby enabling to cover a larger volume with the spectroscopic survey (Eisenstein et al. 2001, 2005). LRGs are passively-evolving, early-type massive galaxies, and their typical ages are estimated as ~ 5 Gyrs (Kauffmann 1996; Wake et al. 2006; Masjedi et al. 2008; Carson & Nichol 2010). This implies that LRGs, at least a majority of the stellar components, were formed at $z \gtrsim 1$ (Masjedi et al. 2008). Motivated by this fact, we here propose a simplest abundance-matching method for connecting LRGs to dark matter distribution in large-scale structure as follows.

Our method rests on an assumption that progenitor halos for LRG-host subhalos today are formed at $z = 2$, which is closer to the peak redshift of cosmic star formation rate (Hopkins & Beacom 2006). Our choice of $z = 2$ is just the first attempt, and a formation redshift can be further explored so as to have a better agreement with the SDSS measurements (see Section 4 and Appendix A for a further discussion). (1) We select halos from the simulation output at $z = 2$ as candidates of the progenitor halos (hereafter sometimes called $z2$ -halo). In doing this, we select the $z2$ -halos in descending order of their masses (from more massive to less massive) until the comoving number density becomes close to that of SDSS LRGs at $z = 0.3$, which we set to $\bar{n}_{\text{LRG}} = 10^{-4} h^3 \text{Mpc}^{-3}$. More precisely, we need to identify more halos having the number density of $\simeq 1.3 \times 10^{-4} h^3 \text{Mpc}^{-3}$ at least, because about 30% of $z2$ -halos, preferentially in massive halo regions at $z = 0.3$, experience mergers from $z = 2$ to $z = 0.3$ for the assumed Λ CDM model (see below for details). (2) We trace the 30% innermost particles of each $z2$ -halo particles to lower-redshift simulation outputs until $z = 0.3$, where the innermost particles are considered as “LRG star” particles and defined by particles within a spherical boundary around the mass peak of each $z2$ -halo (see Figure 1). (3) We perform a matching of the star particles of each $z2$ -halo to central and satellite subhalos at $z = 0.3$ (hereafter $z0.3$ -subhalo). If more than 50% of the star particles are contained in a $z0.3$ -subhalo, we define the subhalo as a subhalo hosting LRG at $z = 0.3$. (4) We repeat this procedure in descending order of masses of $z2$ -halos until the comoving number density of the matched $z0.3$ -subhalos (LRG-host subhalos) is closest to the target value, $\bar{n}_{\text{LRG}} = 10^{-4} h^3 \text{Mpc}^{-3}$. The minimum mass of LRG-progenitor halos at $z = 2$ is about

$6 \times 10^{12} h^{-1} M_{\odot}$ for the L1000 run (which contains about 90 N -body particles for the).

However, we need to a priori determine some model parameters before implementing to the simulation halo/subhalo catalogs: the formation redshift of LRG-progenitor halos, $z_{\text{form}} = 2$, and the fractions “30%” or “50%” for the star particles or the matching particles, respectively. Rather than exploring different combinations of the model parameters to have a better fit to the SDSS measurements, we will below study the ability of our mock catalog to predict various statistical quantities of LRGs, by employing our fiducial choices of the parameters ($z_{\text{form}} = 2$, $f_{\text{star}} = 0.3$ and $f_{\text{match}} = 0.5$). In Appendix A, we study how variations of the model parameters change the mock catalog. The brief summary of the results is the change of each parameter affects only the small-scale clustering signals, which are sensitive to the fraction of satellite LRGs, and does not largely change the clustering signals at large scales in the two-halo regime.

In our method, central and satellite subhalos are populated with LRG galaxies under a *single* criterion: if a subhalo at $z = 0.3$ is a descendant of the $z2$ -halo, the subhalo is included in the matched sample. On the other hand, the standard abundance matching method often uses different mass proxies of central and satellite subhalos when matching subhalos to the target galaxies (in the order of their stellar masses or luminosities). For instance, the mass of a central subhalo is assigned by a maximum circular velocity of the bounded N -body particles, computed from the output at the target redshift ($z = 0.3$ in the LRG case), while the mass of a satellite subhalo is assigned by the maximum circular velocity from the simulation output at the “accretion” epoch before the subhalo started to accrete onto the main host halo (Conroy et al. 2006), which allows one to estimate the mass of each satellite subhalo before being affected by the tidal stripping during penetrating the main halo. Thus the standard abundance matching method is computationally more expensive in a sense that it requires many simulation outputs at different redshifts in order to trace the accretion/assembly history of each subhalo. To be fair, we below compare our method with the standard abundance matching method for some statistical quantities of LRGs.

Some of the LRG-host halos at $z = 0.3$, especially massive halos, contain multiple LRG-subhalos in our mock catalog (see the example in the lower panel of Figure 1). We often call such systems “multiple-LRG systems” in the following discussion (also see Reid & Spergel 2009; Hikage et al. 2012a). We refer to the LRG-host halos, which host only one LRG inside, as “single-LRG systems”. The average halo masses for the single- and multiple-LRG systems are found from the L1000 run to be $\bar{M}_{\text{vir}} = 4.8 \times 10^{13}$ and $1.5 \times 10^{14} h^{-1} M_{\odot}$, respectively. The fraction of the multiple-LRG systems among all the LRG-host halos is about 8% in the L1000 run. Because we assumed that most stars of each LRG are formed until $z = 2$ and the total stellar mass scales with the mass of $z2$ -halo, we define the brightest LRG (BLRG) in each multiple-LRG system by the LRG-subhalo that corresponds to the most massive $z2$ -halo among all the progenitor $z2$ -halos in the system, while we call the smallest $z2$ -halo the faintest LRG (FLRG). Note that we also refer to an LRG in a single-LRG system as BLRG. A BLRG in a single-LRG system is not necessarily a central galaxy in the parent halo at $z = 0.3$ (in other words, the central subhalo does not correspond to any LRG-progenitor halo at $z = 2$). Similarly, a central LRG in a multiple-LRG system is not necessarily a BLRG, i.e. the most massive $z2$ -halo, although the central subhalo is the most massive subhalo in the parent halo by definition.

Table 1 summarizes properties of the LRG-host halos com-

Type of LRG-host halos	Total number	$\bar{M}_{\text{vir}} [10^{13} h^{-1} M_{\odot}]$	$\bar{R}_{\text{vir}} [h^{-1} \text{Mpc}]$	$f_{\text{sat-LRG}}$	$q_{\text{cen}}^{\text{BLRG}}$	$q_{\text{cen}}^{\text{FLRG}}$
All LRG-host halos						
L1000	91,090	5.64 ± 0.11	0.804 ± 0.004	0.0988 ± 0.0054	0.959 ± 0.004	–
L300	2,403	5.66	0.806	0.119	0.956	–
Single-LRG halos						
L1000	83,891	4.81 ± 0.08	0.776 ± 0.004	0.0215 ± 0.0028	0.979 ± 0.003	–
L300	2,166	4.74	0.772	0.0226	0.977	–
Hikage et al. (2012a)	87,889	3.7 ± 0.4	0.77 ± 0.03	0.24 ± 0.18	0.76 ± 0.18	–
Multiple-LRG halos						
L1000	7,199	15.2 ± 0.8	1.13 ± 0.02	1.00	0.735 ± 0.025	0.207 ± 0.023
L300	237	14.0	1.11	1.00	0.764	0.186
Hikage et al. (2012a)	4,157	14.6 ± 1.1	1.21 ± 0.03	1.00	0.63 ± 0.21	0.24 ± 0.13

Table 1. Summary of properties of LRG-host halos, computed from the mock LRG catalog in the L1000 and L300 runs (see text for details). Here we consider all LRG-host halos and the single- and multiple-LRG halos that host only one or multiple LRG(s) inside, respectively. \bar{M}_{vir} and \bar{R}_{vir} are the average virial mass and radius of the host halos (without any weight). $f_{\text{sat-LRG}}$ is the fraction of halos that have satellite LRG(s) among all the LRG-host halos in either single- or multiple-LRG halos (each row). Note that $f_{\text{sat-LRG}}$ for multiple-LRG systems is unity by definition since the halos have satellite LRG(s). $q_{\text{cen}}^{\text{BLRG}}$ is the fraction of halos that host its BLRG as a central galaxy among all the host halos, where BLRG is the brightest LRG, the most massive LRG-progenitor halo at $z = 2$, compared to other LRG-subhalo(s) in the same host halo at $z = 0.3$. Note that, for the single-LRG hosts, we call the LRG as the BLRG. $q_{\text{cen}}^{\text{FLRG}}$ is the fraction of halos that host FLRG as a central LRG, where FLRG is the faintest LRG, the smallest LRG-progenitor halo, in each multiple-LRG halo. The error bars quoted for the L1000 mock are the standard deviation computed from the 27 divided sub-volumes of L1000 mock each of which has volume of $333^3 [h^{-1} \text{Mpc}]^3$. Hence, the L1000 results with the errors in each row can be compared with the L300 mock results, which has comparable volume of $300^3 [h^{-1} \text{Mpc}]^3$. For comparison, we also quote the measurement results derived from the SDSS DR7 LRG catalog in Hikage et al. (2012a), where the error bars are $\pm 68\%$ confidence ranges (see text for details).

puted from the L1000 and L300 mock catalogs. To estimate statistical uncertainties of each quantity, we divided the L1000 catalog into 27 sub-volumes (the side length of each sub-volume is $333 h^{-1} \text{Mpc}$) and computed the mean and rms of the quantity¹¹. Hence the error quoted for each entry of the L1000 run corresponds to the sample variance scatter for a volume of $[333 h^{-1} \text{Mpc}]^3$. The L1000 result with the error bar can be compared with the L300 result, because of the similar volumes of the sub-divided L1000 catalog and L300 run (333^3 and $300^3 [h^{-1} \text{Mpc}]^3$, respectively). The L1000 and L300 results agree with each other to within 2σ for the quantities except for the fraction of satellite LRGs for all the LRG-host halos. The disagreement for the satellite LRG fraction is probably due to the numerical resolution, because the L1000 simulation may miss some less-massive LRG progenitor-halos at $z = 2$, which are identified in the L300 run, due to lack of the numerical resolution and such small $z = 2$ -halos preferentially become satellite LRGs at $z = 0.3$ (also see below and Appendix A).

In Table 1, we also compare the mock results with the measurement results from the SDSS DR7 LRG catalog in Hikage et al. (2012a). The SDSS results were derived using the different clustering measurements, the LRG-galaxy lensing, the LRG redshift-space power spectrum, and the LRG-photometric galaxy cross-correlation to constrain the properties of LRG-host halos. To be conservative, we here quote the measurement result that has largest uncertainties among the three measurements. The table shows that the mock catalog fairly well reproduces the SDSS results within the error bars. Although one may notice sizable disagreement for the single-LRG systems, especially for the fraction of halos hosting satellite LRGs ($f_{\text{sat-LRG}}$) or the fraction of central BLRGs ($q_{\text{cen}}^{\text{BLRG}}$), the SDSS measurements are not yet reliable for the single-LRG systems, as reflected by the large error bars

¹¹ Note that, when computing the mean value from the 27 sub-volume catalogs, we did not use any weight, e.g. by halo mass. For this reason, the relation, $\bar{M}_{\text{vir}} = 4\pi\bar{\rho}_{m0}\Delta_{\text{vir}}\bar{R}_{\text{vir}}^3/3$, does not hold for the mean halo mass and the mean virial radius for the LRG-host halos in Table 1.

and stressed in Hikage et al. (2012a). Hence, this requires a further careful study.

Figure 1 shows snapshots of the N -body particle distribution in the L1000 run outputs at different redshifts, for the regions where multiple- or single-LRG systems are formed at $z = 0.3$. The figure illustrates how each LRG-progenitor halo is defined at $z = 2$, how the innermost particles are assigned as “star” particles, and how the star particles are traced to lower redshifts and how LRG-progenitor halos merge with each other and become to reside in central and satellite subhalos at the final redshift $z = 0.3$. Our method allows us to directly include the merging and assembly histories of LRG-progenitor halos. Although the number density of LRG-host subhalos is set to the density of LRGs as we described above, the figure shows that more LRG-progenitor halos or subhalos survive at higher redshift than at $z = 0.3$. Hence our method has a capability to study what kinds of halos or subhalos at higher redshift are progenitors for the SDSS LRGs (see Section 4 for a further discussion).

Figure 2 shows how each LRG-progenitor halo at $z = 2$ loses or gains its mass due to mass accretion, merger and/or tidal stripping when it becomes an LRG-host subhalo at $z = 0.3$, computed using the catalogs of halos and subhalos in the $z = 2$ and $z = 0.3$ outputs of L1000 run. Note that the halo mass shown in the x -axis, $M_{\text{FoF}}(z = 2)$, is the FoF mass, the sum of FoF particles in each halo region at $z = 2$. First, the figure shows that we need to select the LRG-progenitor halos at $z = 2$ down to a mass scale of about $6 \times 10^{12} h^{-1} M_{\odot}$. Some subhalos for satellite LRGs lose their masses due to tidal stripping as implied in Figure 1, while subhalos for central LRGs gain their masses due to mass accretion and/or merger. Comparing the left and right panels manifests that multiple-LRG systems tend to reside in more massive LRG-progenitor halos at $z = 2$ and become more massive LRG-host halos at $z = 0.3$, and that the mass difference between subhalos for central and satellite LRGs is larger in multiple-LRG systems, implying a larger difference between their luminosities (see Hikage et al. 2012a, for a similar discussion).

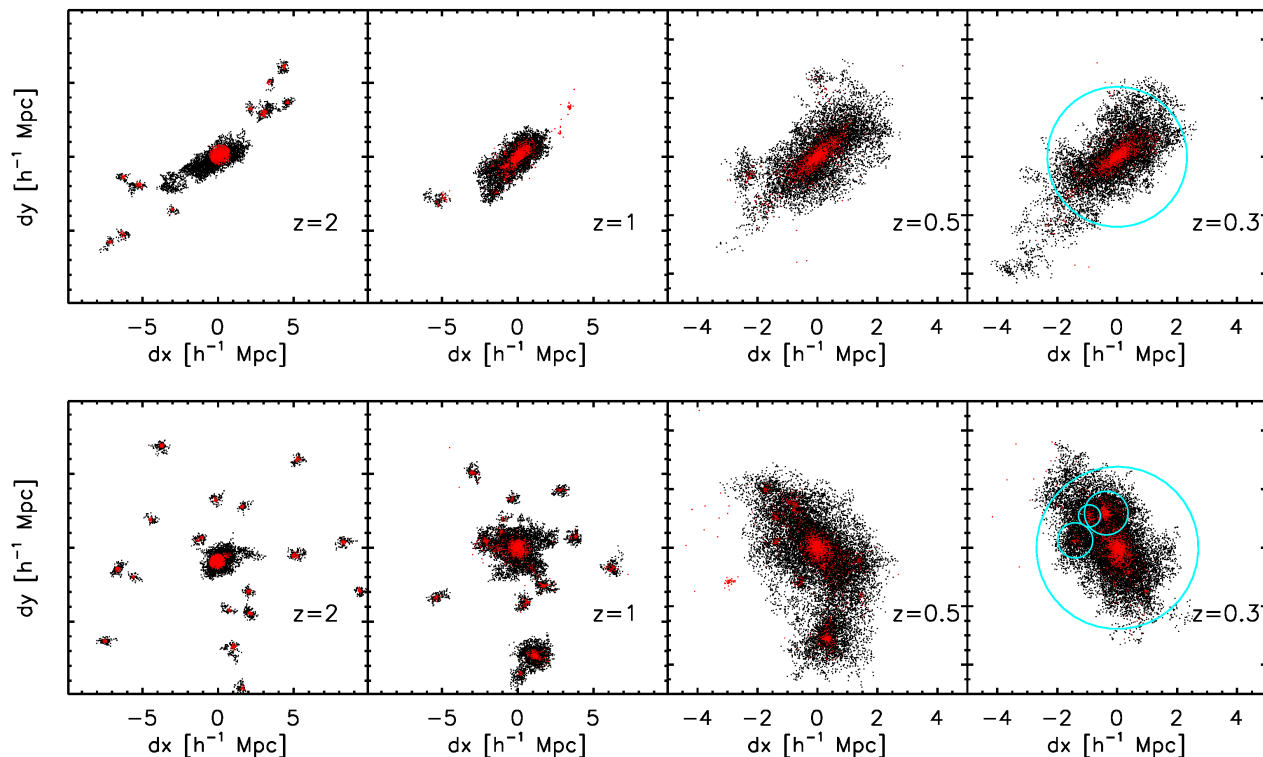


Figure 1. Evolution of dark matter (N -body) particle distribution around the region of subhalos hosting mock LRGs at $z = 0.3$, taken from our L1000 simulation run. The upper-row panels are for the region around the host-halo of the brightest LRG among single-LRG systems (the host halo mass $M_{\text{vir}} = 8.42 \times 10^{14} h^{-1} M_{\odot}$), systems which host only single LRG inside in the $z = 0.3$ output, while the lower-row panels are the most massive host-halo among systems hosting one central and three satellite LRGs ($M_{\text{vir}} = 1.44 \times 10^{15} h^{-1} M_{\odot}$). The dot symbols in each panel are member particles in the halo regions at $z = 2$ or the subhalo region(s) at lower redshifts. The red-color particles are 30% innermost particles of each halo at $z = 2$ and selected based on our abundance matching method between the progenitor halos and the LRG-host subhalos at $z = 0.3$ to reproduce the observed number density of SDSS LRGs (see text for details). Then we trace where the red-color particles are distributed in each subhalo region at lower redshift. By matching the red-color particles to central and satellite subhalos in each host halo of $z = 0.3$ output, we can define locations of each LRG in a host halo at $z = 0.3$; if a subhalo at $z = 0.3$ contains more than 50% of the red-color particles of a progenitor halo, we define it as an LRG-host subhalo. The upper-row panels show the case that 11 progenitor halos of LRGs are formed at $z = 2$, and then are merged at lower redshift, forming one central LRG in the host halo at $z = 0.3$. The lower-row panels show that 24 progenitor halos at $z = 2$ form one central LRG and three satellite LRGs in the host-halo at $z = 0.3$. The blue circles in the panel of $z = 0.3$ shows the positions of mock LRGs. The size of each circle is proportional to $M_{\text{sub}}^{1/3}$, where M_{sub} is the subhalo mass.

Thus our method is primarily based on the masses of LRG-progenitor halos at $z = 2$ (see Figure 2) and the connection with central and satellite subhalos in the parent halos at $z = 0.3$. On the other hand, LRGs in the SDSS catalog are selected based on the magnitude and color cuts from the SDSS imaging data (primarily gri), and are not necessarily a stellar-mass-selected sample, although their stellar masses are believed to have a tight relation with the host halo masses. Nevertheless, we will show below that the mock catalog perhaps surprisingly well reproduces the different SDSS measurements.

Since LRGs in our mock catalog reside in relatively massive halos at $z = 2$, with masses $M_{\text{FoF}} \gtrsim 6 \times 10^{12} h^{-1} M_{\odot}$ (Figure 2), as well as in massive parent halos at $z = 0.3$, our method does not necessarily require a high-resolution simulation. A simulation with 1024^3 particles and $1 h^{-1} \text{Gpc}$ size on a side seems sufficient, which allows for a relatively fast computation of the N -body simulation as well as an accurate estimation of statistical quantities of LRGs. This is not the case if one wants to work on the abundance matching method for less massive galaxies or more general types of galaxies (e.g., Trujillo-Gomez et al. 2011; Reddick et al. 2012; Masaki et al. 2013).

3 RESULTS: COMPARISON WITH THE SDSS LRG MEASUREMENTS

3.1 Halo occupation distribution and properties of satellite LRGs

First, we study the halo occupation distribution (HOD) for LRGs in Figure 3, where the HOD gives the average number of LRGs that the halos at $z = 0.3$ host as a function of host-halo mass. Here we consider the HODs for central and satellite LRGs which reside in central and satellite subhalos in the LRG-host halos, respectively. Again we should emphasize that our method does not assume any functional forms for the HODs, unlike done in the standard HOD method, and rather allows us to directly compute the HODs from the mock catalog. Even if LRG-progenitor halos are selected from halos at $z = 2$ by a *sharp* mass threshold, our mock catalog naturally predicts that the central HOD has a smoother shape around a minimum halo mass, as a result of their merging and assembly histories from $z = 2$ to $z = 0.3$. To be more precise, the central HOD is smaller than unity ($\langle N_{\text{cen}} \rangle < 1$) for host halos with $M_{\text{vir}} \lesssim 10^{14} h^{-1} M_{\odot}$, meaning that only some fraction of the halos host a central LRG. On the other hand, most of massive halos

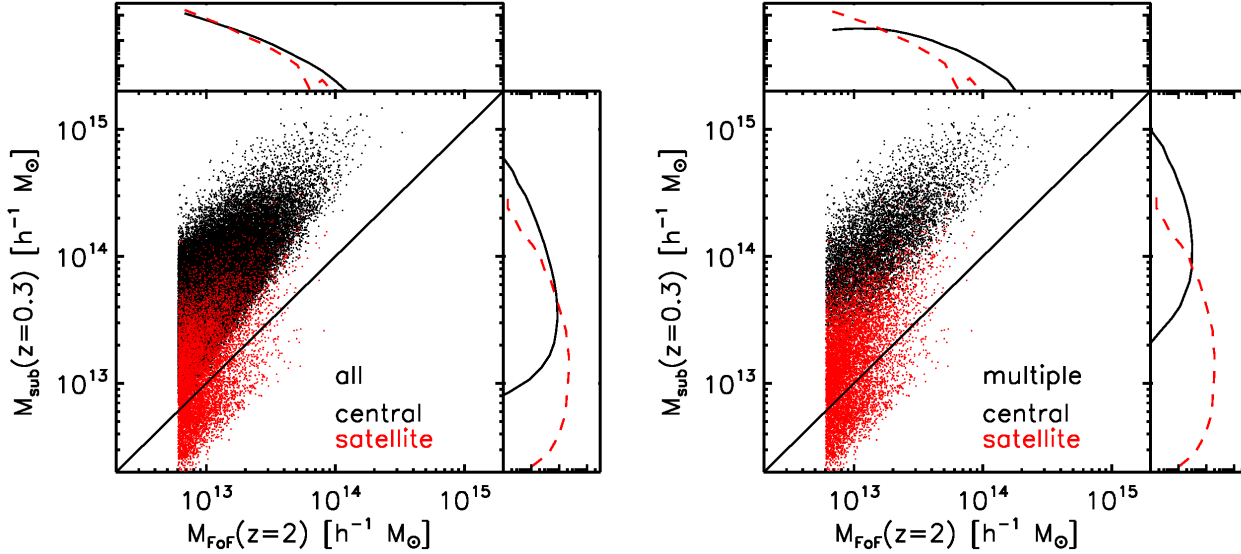


Figure 2. Comparison between masses of the LRG-progenitor halos at $z = 2$ and the LRG-host subhalos at $z = 0.3$, computed from the L1000 run, where each progenitor halo and subhalo are matched based on our method (see Figure 1). The left and right panels show the results for all the LRG-host halos and the multiple-LRG systems, respectively. The black and red points are for central and satellite LRGs, respectively. Note that the central LRG-subhalo is a smooth component of the parent halo at $z = 0.3$. The line in each panel shows the case that the progenitor halo does not either gain or lose its mass at $z = 0.3$: $M_{\text{sub}}(z = 0.3) = M_{\text{FoF}}(z = 2)$. The figure shows that satellite LRGs preferentially reside in less massive progenitor halos at $z = 2$, some subhalos for satellite LRGs lose their masses due to tidal stripping when accreting into more massive halos, and subhalos for central LRGs gain their masses due to merger. The upper- and right-side panels in each plot are the projected distributions for central and satellite LRGs along the y - or x -axis direction, respectively.

host at least one LRG and can host multiple LRGs inside. Conversely, the fraction of massive halos, which do *not* host *any* LRG, is 1.3% for halos with masses $M_{\text{vir}} \geq 1 \times 10^{14} h^{-1} M_{\odot}$, while *all* halos with $M_{\text{vir}} \geq 2 \times 10^{14} h^{-1} M_{\odot}$ have at least one LRG inside.

To test validity of our mock catalog, we compare the HODs with the SDSS measurement in Reid & Spergel (2009, hereafter RS09), where the HOD was constrained by using the Counts-in-Cylinders (CiC) method for identifying multiple LRG systems from the SDSS DR7 LRG catalog with the aid of halo catalogs in N -body simulations. Although RS09 employed the slightly different cosmological model and redshift ($z = 0.2$) from ours ($z = 0.3$), we employed the same best-fit parameters in RS09 to compute the LRG HOD for this figure. To be more precise, due to limited constraints from the SDSS LRG catalog, especially for low-mass host-halos, RS09 assumed the fixed form for the central HOD:

$$\langle N_{\text{cen}}(M) \rangle = \frac{1}{2} \left[1 + \text{erf} \left(\frac{\log M - \log M_{\text{min}}}{\sigma_{\log M}} \right) \right], \quad (1)$$

with $M_{\text{min}} = 5.7 \times 10^{13} h^{-1} M_{\odot}$ and $\sigma_{\log M} = 0.7$, in order to obtain meaningful constraints on the satellite HOD. The central HOD for low-mass host-halos is difficult to constrain, because low-mass host-halos of LRGs are observationally difficult to identify. Therefore, we do not think that the difference for the central HODs is significant, and needs to be further carefully studied.

On the other hand, the satellite HOD in RS09 is almost perfectly recovered by our mock catalog, where RS09 assumed the functional form for the satellite HOD to be given by $\langle N_{\text{sat}}(M) \rangle = \langle N_{\text{cen}}(M) \rangle [(M - M_{\text{cut}})/M_1]^\alpha$ and then constrained the parameters ($M_{\text{cut}}, M_1, \alpha$) from the SDSS LRG catalog. The hatched region is the range at each host-halo mass bin that is allowed by varying the model parameters within the 1σ confidence regions. Our results confirm that parent halos of $\sim 10^{15} h^{-1} M_{\odot}$ have up to

several LRGs inside, as first pointed out in RS09. The L300 result, the simulation result with higher spatial resolution, gives similar results to the L1000 results, showing that the numerical resolution is not an issue in studying the satellite HOD. Even though SDSS LRGs are selected by the magnitude and color cut, not by their masses, our method seems to capture the origin of SDSS LRGs; mass-selected halos at $z \sim 2$ are main progenitors of LRGs, and their subsequent assembly and merging histories determine where LRGs are distributed within the host halos at lower redshift.

Furthermore, to be comprehensive, we also compare our method with the standard abundance matching method in Conroy et al. (2006). In this method, the mass proxy of each subhalo is assigned by the maximum circular velocity V_{cir} computed from the member N -body particles. More specifically, the central subhalo mass is assigned by V_{cir} at the LRG redshift $z = 0.3$, while the satellite subhalo mass is estimated by V_{cir} from the simulation output at its ‘‘accretion’’ epoch when the subhalo started to accrete onto the parent halo at $z = 0.3$ (more exactly, the circular velocity is estimated from the last output when the ‘‘subhalo’’ was identified as an ‘‘isolated’’ halo before the accretion) (see also Masaki et al. 2013). This prescription for satellite subhalos allows for a better assignment of the subhalo mass so that it avoids the effect by tidal stripping during accreting onto the parent halo. We use the L300 run outputs at 44 different redshifts from $z = 10$ to trace the merging and assembly history of each subhalo till $z = 0.3$. Then, assuming that the stellar masses of LRGs trace the subhalo masses, we match the $z = 0.3$ subhalos to LRGs in descending order of the mass proxies (V_{cir}) until the number density is closest to the target value, $\bar{n}_{\text{LRG}} = 10^{-4} (h \text{ Mpc}^{-1})^3$. The curves labeled as ‘‘Standard (V_{acc})’’ show the central and satellite HODs measured from the mock catalog of the V_{cir} -based abundance matching method. The satellite HOD is in a nice agreement with our method, while the central HOD from the abundance matching method displays a

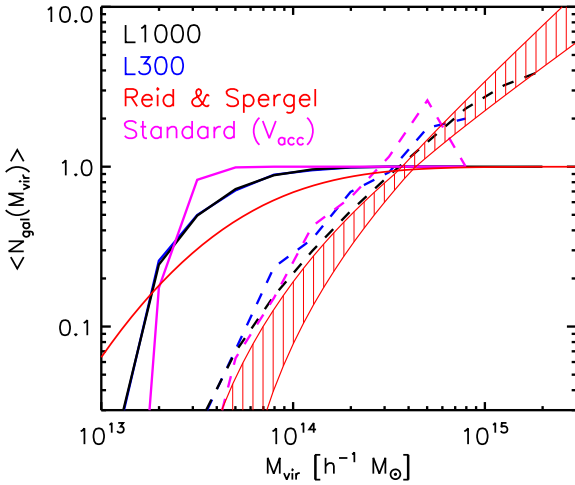


Figure 3. The halo occupation distribution (HOD) for LRGs as a function of parent halo mass, measured from our mock catalog. Our mock catalog has an assignment of each LRG to central or satellite subhalos in a parent halo at $z = 0.3$ (see Figure 1), thereby allowing us to compute the HODs for central (solid curve) and satellite (dashed) LRGs. The black and blue curves are the results from the L1000 and L300 runs, respectively, where the L300 run is a higher resolution run with a small box size, $300 h^{-1} \text{Mpc}$ (see text for details). The red curves show the SDSS measurements, taken from Reid & Spergel (2009, RS09). RS09 fixed the function form of central HOD, and then constrained the satellite HOD from the SDSS LRG catalog using the Counts-in-Cylinders technique. The hatched region is the range allowed by varying each model parameter of the satellite HOD within its 1σ confidence range. The mock catalog well reproduces the SDSS measurements, including the shape of central HOD around the cutoff mass scale as well as the slope and amplitude of satellite HOD, without employing any free parameter to adjust after the abundance matching. The magenta lines show the HODs from the LRG mock catalog generated using the standard abundance matching method in Conroy et al. (2006) (also see text for the details).

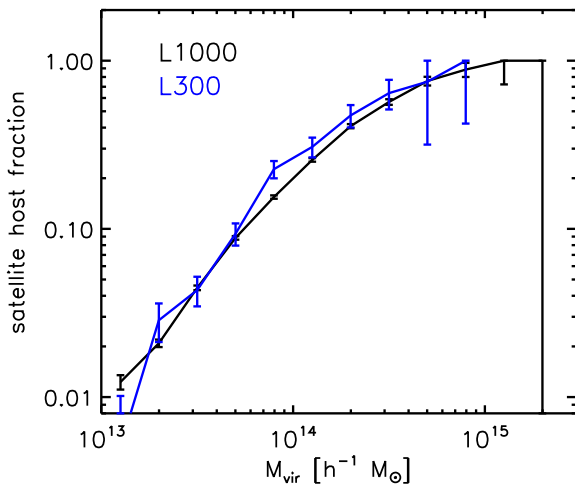


Figure 4. The fraction of halos hosting *satellite* LRG(s) inside as a function of halo mass, computed by using all the LRG-host halos at $z = 0.3$ in the L1000 and L300 runs.

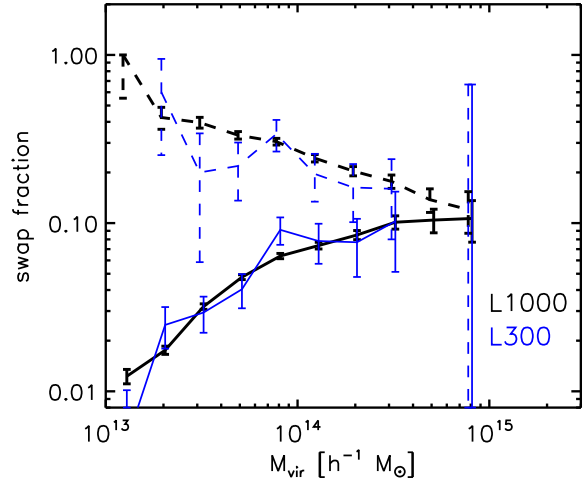


Figure 5. The solid curves show the fraction of the parent halos hosting the brightest LRG (BLRG) as a *satellite* galaxy, among all the LRG-host halos. Here the BLRG is the most massive LRG-progenitor halo at $z = 2$ among all the progenitor halos which become to reside in the same LRG-host halo at $z = 0.3$. The dashed curves are the similar fraction of LRG-host halos with satellite BLRG, but computed using only the multiple-LRG systems. The error bars are computed from the number of halos in each mass bin assuming Poisson statistics.

sharper cut-off than in our method. Again we do not yet know the genuine cut-off feature of the central HOD due to lack of the measurement constraints. We will below further compare our method with the abundance matching method for other statistical quantities of LRGs.

One motivation of this paper is to understand the physics of the nonlinear redshift-space distortion, i.e. the Finger-of-God (FoG) effect, in the redshift-space power spectrum of LRGs. The FoG effect is caused by internal motion of satellite LRG(s) in LRG-host halos (Hikage et al. 2012b,a). In the following, we study several quantities relevant for the FoG effect; the fraction of satellite LRGs, the radial profile of satellite LRGs inside the parent halos and the internal velocities of satellite LRGs (see Hikage et al. 2012b, for details of the theoretical modeling).

Figure 4 shows how much fraction of LRG-host halos at $z = 0.3$ host *satellite* LRG(s) inside, as a function of the halo mass. Note that we excluded halos that do not host any LRG in this statistics, but included the single-LRG systems hosting one LRG as a *satellite* galaxy when computing the numerator of the fraction (in this case, the central subhalo of the parent halo does not correspond to any LRG-progenitor halo at $z = 2$). The error bars around the solid curve are Poisson errors, estimated using the number of halos in each mass bin. The figure shows that more massive halos have a higher probability to host satellite LRG(s). About 20% of parent halos with $M_{\text{vir}} \simeq 10^{14} h^{-1} M_{\odot}$ host satellite LRG(s).

We naively expect that BLRG, the most massive LRG-progenitor halo at $z = 2$ among LRG-progenitor halo(s) accreting onto the same parent halo at $z = 0.3$, becomes a central galaxy. The solid curves in Figure 5 show the fraction of BLRGs to be a satellite galaxy in LRG-host halos at $z = 0.3$ as a function of the halo mass, computed using all the LRG-host halos. For halos with $M_{\text{vir}} \gtrsim 10^{14} h^{-1} M_{\odot}$, there is up to 10% probability for its BLRG to be a satellite galaxy.

The dashed curves are the similar fraction, but computed us-

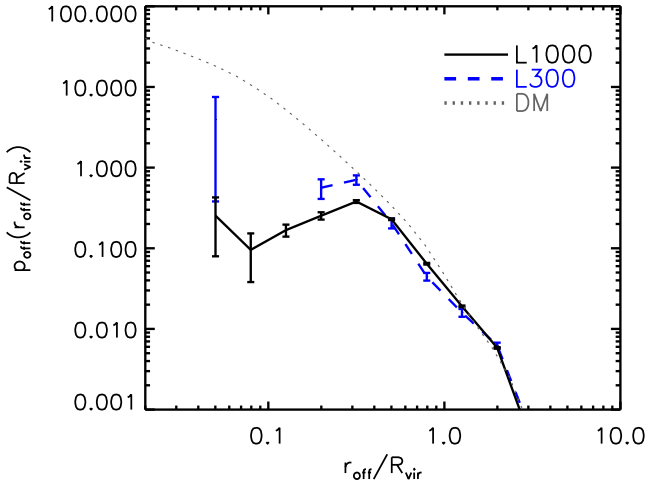


Figure 6. The average radial profile of satellite LRG host subhalos, obtained by stacking the positions of satellite LRGs in all the LRG-host halos with satellite LRG(s), as a function of radius relative to the virial radius of each parent halo. The mean mass of the LRG-halos used in this calculation is $M_{\text{vir}} \simeq 1.31$ or $1.24 \times 10^{14} h^{-1} M_{\odot}$ for the L1000 or L300 runs, while the mean virial radius is $R_{\text{vir}} \simeq 1.07$ or $1.06 h^{-1} \text{Mpc}$, respectively. For comparison, the upper dotted curve shows the profile of dark matter averaged for the same host halos with an arbitrary amplitude. The error bars at each radial bin are estimated by first dividing LRG-host halos into 27 subsamples (27 subvolumes) and then computing variance of the number of satellite LRGs at the radial bin. The typical off-center radius for satellite LRGs appears to be about $400 h^{-1} \text{kpc}$.

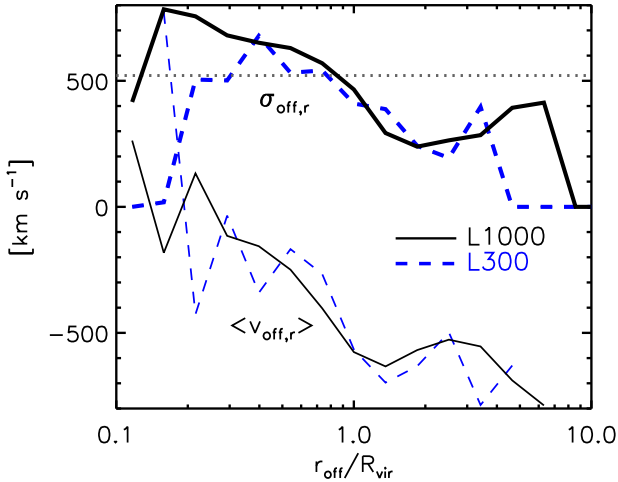


Figure 7. The average radial velocity of satellite LRGs, $\langle v_{\text{off},r} \rangle$, with respect to the halo center in each LRG-host halo, computed by using all the LRG-host halos with satellite LRG(s) as in the previous figure. The negative $\langle v_{\text{off},r} \rangle$ means a coherent infall towards the halo center. The upper curves show the average radial velocity dispersion around the coherent infall, $\sigma_{\text{off},r}$. For the comparison, the dotted line shows the average velocity dispersion expected from virial theorem, $\sigma_{\text{vir}} = \sqrt{GM_{\text{vir}}/2R_{\text{vir}}}$. The combination of $\langle v_{\text{off},r} \rangle$ and $\sigma_{\text{off},r}$ implies that satellite LRG(s) sink towards the halo center due to dynamical friction, and then have an oscillating motion around the halo center with the velocity dispersion of $\simeq 500 \text{ km s}^{-1}$.

ing only the multiple LRG systems. This sample is intended to compare with the recent result in Hikage et al. (2012a) (also see Table 1). In this case, the fraction of satellite BLRGs is higher for host halos with smaller masses, with larger error bars. This can be explained as follows. Most of low-mass host-halos with masses $\lesssim 10^{14} h^{-1} M_{\odot}$ are single-LRG systems as can be found from Figure 3, and only a small number of such halos are multiple-LRG systems, causing larger Poisson error bars at each mass bin. We have found from the simulation outputs that such low-mass halos of multiple LRG systems (mostly the systems with 2 LRGs) tend to display a bimodal mass distribution due to ongoing or past major merger, where the BLRG and other (mostly central) LRG tend to have the small mass difference. As a result, such low-mass multiple-LRG systems have a higher chance to host the BLRG as a satellite LRG. On the other hand, the fraction of halos with satellite BLRG converge to the solid curve with increasing the host-halo mass, because most of such massive halos are multiple-LRG systems. For multiple LRG systems with mass of $M_{\text{vir}} \simeq 10^{14} h^{-1} M_{\odot}$, about 30% of BLRGs are satellite galaxies.

Recently, Hikage et al. (2012a) studied the multiple-LRG systems defined from the SDSS DR7 catalog by applying the CiC technique as well as the FoF group finder method to the distribution of LRGs in redshift space. Then they used the different correlation measurements, the redshift-space power spectrum, the LRG-galaxy lensing and the cross-correlation of LRGs with photometric galaxies, to study properties of satellite LRGs. From the lensing analysis, they found that the multiple-LRG systems has a typical halo mass of $M_{\text{vir}} \simeq 1.5 \times 10^{14} h^{-1} M_{\odot}$ (with a roughly 10% statistical error), and that $37 \pm 21\%$ of BLRGs in the multiple-LRG systems appear to be satellite galaxies¹². Our mock catalog shows a fairly good agreement with the SDSS results, for the average halo mass and the fraction of satellite BLRGs (also see Table 1).

In Figure 6, we study the average radial profile of satellite LRGs. In this calculation, we employ only the host halos containing satellite LRG(s), and estimate the radial profile by stacking the radial distribution of satellite LRG(s) in units of the radius relative to the virial radius of each halo. We use the mass peak of the smooth component as the halo center. The average profile p_{off} is normalized as

$$\int dr' 4\pi r'^2 p_{\text{off}}(r') = 1, \quad \text{with } r' = r_{\text{off}}/R_{\text{vir}}, \quad (2)$$

where r_{off} is the distance from the density maximum of the smooth component. The average mass of the host halos is $M_{\text{vir}} \simeq 1.31 \times 10^{14}$ or $1.24 \times 10^{14} h^{-1} M_{\odot}$ for the L1000 or L300 run, respectively, while the average virial radius $R_{\text{vir}} \simeq 1.07$ or $1.06 h^{-1} \text{Mpc}$ in the comoving unit. Compared to the dark matter profile, the radial profile of satellite LRGs clearly displays a flattened profile. The typical off-center radius, where the profile starts to be flattened, is found to be about $400 h^{-1} \text{kpc}$ because $R_{\text{vir}} \simeq 1 h^{-1} \text{Mpc}$, which is in a good agreement with the result for the multiple systems in Hikage et al. (2012a). The radial profile also shows a decline at the smaller radii. Thus our result is not consistent with the assumption often used in a standard HOD method that the radial profile of member galaxies follows the dark matter profile (see Berling & Weinberg 2002, for the improved HOD method including a possible variation in the radial profile of member galax-

¹² Note that Hikage et al. (2012a) used the halo mass definition of M_{180b} instead of the virial mass M_{vir} in their analysis, where M_{180b} is defined by the enclosed mass inside which the mean density is 180 times the mean background mass density.

ies). However, the L300 run shows no satellite LRG at small radii $r_{\text{off}}/R_{\text{vir}} \leq 0.1$, except for the innermost bin. Thus the satellite LRGs at the small radii are mainly from most massive host-halos, which do not exist in the smaller box simulation, L300. Although the mock catalogs show a sharp rise at the innermost bin $r_{\text{off}}/R_{\text{vir}} \simeq 0.06$ ($r_{\text{off}} \simeq 60 h^{-1} \text{kpc}$), which may indicate merging LRGs to the central subhalo in the less massive halos, the scatters are large even for the L300 run, so the result is not significant. Nevertheless, it is worth mentioning that the satellite LRG distribution in our mock catalog seems to show a similar profile to the profile of most massive subhalos in cluster-scale halos in Gao et al. (2012) (see Figures 15 and 16 for the profile). These features in the radial profile of massive subhalos may be as a result of dynamical friction, tidal stripping and merger to the central subhalo. However, the L300 and L1000 results show some difference at the small scales, so a further careful study is needed to derive a more robust conclusion, by using high-resolution simulations as well as a larger number of the realizations.

Figure 7 shows the average radial profile of internal motions of satellite LRGs in the parent halos, where the bulk motion of each parent halo (the average velocity of N -body particles belonging to the smooth component of the halo) is subtracted from the velocity of each LRG-host subhalo. We considered only the host halos with satellite LRG(s) as in Figure 6. The curves, labelled as $\langle v_{\text{off},r} \rangle$, are the average radial velocities for all the satellite LRGs with respect to the halo center. The average velocity is negative, reflecting the coherent infall motion towards the halo center, and the infall velocity is larger with increasing radius up to the virial radius. The average radial velocity becomes zero on average at the halo center. These support that the LRG-host subhalo approaches to the halo center due to dynamical friction. On the other hand, the curves, labelled as $\sigma_{\text{off},r}$, are the average velocity dispersions of satellite LRGs. The velocity dispersion has greater amplitudes with decreasing the radius, reaching to $\sigma_{\text{off},r} \simeq 500 \text{ km s}^{-1}$. For comparison, the horizontal dotted line shows the average virial velocity dispersion, $\sigma_{\text{vir}} \equiv \sqrt{GM_{\text{vir}}/2R_{\text{vir}}} = 521 \text{ km s}^{-1}$, among the satellite LRG-host halos in the L1000 run. The combination of $\langle v_{\text{off},r} \rangle$ and $\sigma_{\text{off},r}$ implies that satellite LRGs gradually approach to the halo center due to dynamical friction and have an oscillating motion around the halo center. Again the amplitude of the velocity dispersion, $\sigma_{\text{off},r} \simeq 500 \text{ km s}^{-1}$, is in nice agreement with the recent measurement in Hikage et al. (2012a), where they found the velocity dispersion of about 500 km s^{-1} for satellite LRGs in the multiple-LRG systems by combining the different correlation measurements from the SDSS DR7 LRGs. In Section 3.4 we will further discuss how satellite LRG-subhalos affect the redshift-space power spectrum due to the FoG effect.

3.2 Projected correlation function

Next we study the projected auto-correlation function of LRGs, $w_p(R)$, defined as

$$w_p(R) = 2 \int_0^{\pi_{\text{max}}} d\pi \xi_{gg}(r = \sqrt{\pi^2 + R^2}), \quad (3)$$

where R is the projected separation between two LRGs in the pairs used for the correlation measurement in units of the comoving scale, π is the separation parallel to the line-of-sight and $\xi_{gg}(r)$ is the three-dimensional correlation function. Following Zehavi et al. (2005), π_{max} is set to be $80 h^{-1} \text{Mpc}$. The projected correlation function is not affected by the redshift-space distortion effect due to peculiar velocities of LRGs.

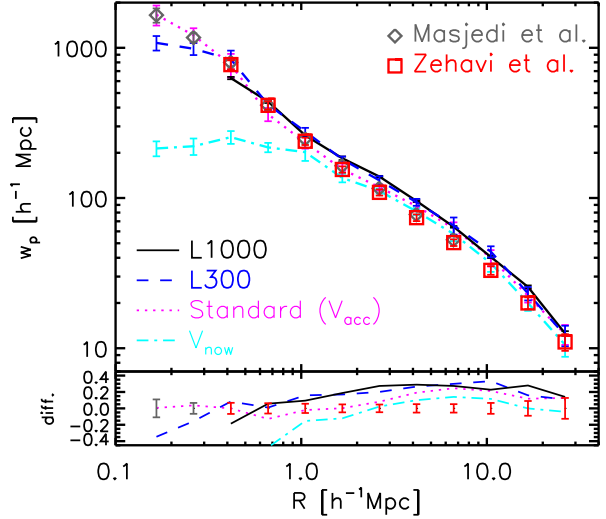


Figure 8. *Top panel:* Projected auto-correlation function of LRGs, $w_p(R)$, as a function of the projected distance R . The solid and dashed curves show the results from our mock catalogs in the L1000 and L300 runs, respectively. The error bars are estimated using the measurements from 8 subdivided volumes of each simulation volume, where the error bars are estimated by dividing the standard deviation by $\sqrt{8}$. Hence the error bars are the statistical scatters for a volume of $(1 h^{-1} \text{Gpc})^3$ or $(300 h^{-1} \text{Mpc})^3$, respectively. The square and diamond symbols are the correlation functions measured from the SDSS catalog of LRGs at $z \sim 0.3$, taken from Zehavi et al. (2005) and Masjedi et al. (2006), respectively. For comparison, the magenta, dotted curve shows the result from the standard abundance matching method as in Figure 3. Furthermore, we also show the prediction obtained if we used the maximum circular velocity at the LRG redshift $z = 0.3$, instead of the accretion epoch, for the satellite subhalos in the abundance matching method (see text for the details). *Bottom panel:* The fractional differences of the model predictions compared to the SDSS measurements.

In Figure 8, we compare the projected correlation function measured from our LRG mock catalog with the SDSS measurements (Zehavi et al. 2005; Masjedi et al. 2006). In the SDSS measurements, Zehavi et al. (2005) used an LRG sample in the magnitude range of $-23.2 < M_g < -21.2$ and with the mean redshift $\langle z \rangle \simeq 0.3$. Masjedi et al. (2006) used the same sample to extend the measurement down to very small scale, below $R = 500 h^{-1} \text{kpc}$, by taking into account various observational effects such as the fiber collision. Note that the cosmological model employed in the measurement is slightly different from the model we assumed for our simulations. The figure shows that our mock catalog remarkably well reproduces the projected correlation function of LRGs, to within 30% accuracy in the amplitude, over a wide range of separation radii, which arise from correlations between LRGs within the same host halo and in different host halos, the so-called one- and two-halo regimes, respectively¹³. Comparing the results for the L1000 and L300 runs reveals that the correlation function for L1000 has a smaller amplitude at $R < 0.7 h^{-1} \text{Mpc}$ than that for L300. Thus the L1000 run implies a systematic error due to the lack of numerical resolution at the small scales. The L300 result shows a better agreement with the SDSS measurement in Masjedi et al. (2006). The small-scale clustering arises mostly from correlation

¹³ Note that the error bars for the mock catalogs are estimated in a different way from those in Table 1, and the error bars in Figures 8 – 10 are the statistical scatter for a volume of $(1000 h^{-1} \text{Gpc})^3$ or $(300 h^{-1} \text{Mpc})^3$.

between LRGs in the same multiple-LRG system, so that numerical resolution seems important to resolve these small subhalos (also see below for a further discussion).

As in Figure 3, the dotted curve gives the result from the standard abundance matching method, which shows almost similar-level agreement with the SDSS measurements to our method. Thus, since the abundance matching method rests on the higher-resolution L300 outputs at 44 different redshifts (in our case), our method can provide a much computationally-cheap, alternative approach to making a mock catalog of LRGs. Furthermore, for comparison, the dot-dashed curve shows the correlation function, if the abundance matching is done by using the maximum circular velocity at the LRG redshift ($z = 0.3$) for each satellite subhalo as its mass proxy, instead of the velocity at the accretion epoch. The result shows a significant discrepancy with the SDSS measurements or our method and the standard abundance matching method, especially at small radii. The disagreement means that the circular velocity at $z = 0.3$ is not a good mass proxy for satellite subhalos when matching the subhalos to LRGs, because it misses satellite subhalos in the multiple-LRG systems. To be more precise, mass (circular velocity) of each satellite subhalo tends to be underestimated due to the tidal stripping, then tends to be not selected by the abundance matching, and instead other isolated, less-massive halos tend to be selected. This reduces the clustering signals at small scale due to less contribution from satellite subhalos and also reduces the clustering signal at large scales due to a smaller bias for such low-mass halos. Thus detailed features of the correlation functions at different scales are sensitive to the contribution of satellite LRGs as well as the low-mass threshold of central HOD in Figure 3 (also see Appendix A). Note that an explicit implementation of the abundance matching method to LRGs is the first time, and the result in Figure 8 highlights the importance of proper assignment of subhalo masses in the abundance matching method.

3.3 LRG-galaxy weak lensing

Correlating the positions of LRGs with shapes of background galaxies, the so-called LRG-galaxy weak lensing, is a powerful means of probing the average dark matter distribution around the LRGs (Mandelbaum et al. 2006, 2012). The LRG-galaxy lensing measures the radial profile of differential surface mass density defined as

$$\Delta\Sigma(R) = \bar{\Sigma}(< R) - \Sigma(R). \quad (4)$$

The profile $\Sigma(R)$ is the average surface mass density around the LRGs defined as

$$\Sigma(R) = \bar{\rho}_{m0} \int d\pi [1 + \xi_{gm}(r = \sqrt{\pi^2 + R^2})], \quad (5)$$

where $\bar{\rho}_{m0}$ is the mean background mass density today, and $\xi_{gm}(r)$ is the three-dimensional cross-correlation between LRGs and the surrounding matter. In Eq. (4), $\bar{\Sigma}(< R)$ is the surface mass density averaged within a circular aperture of a radius R . Our use of the mean mass density today ($\bar{\rho}_{m0}$) is due to our use of the comoving units.

Figure 9 shows that the average mass profile measured for all LRGs in the mock catalog is in good agreement with the SDSS measurement in Mandelbaum et al. (2012), to within 30% level in the amplitude. Note that, to obtain the average mass profile from our mock catalog, we stacked all N -body particles around all the LRG-host subhalo in the simulation, including the particles outside dark matter halos. The lensing signal at the radii

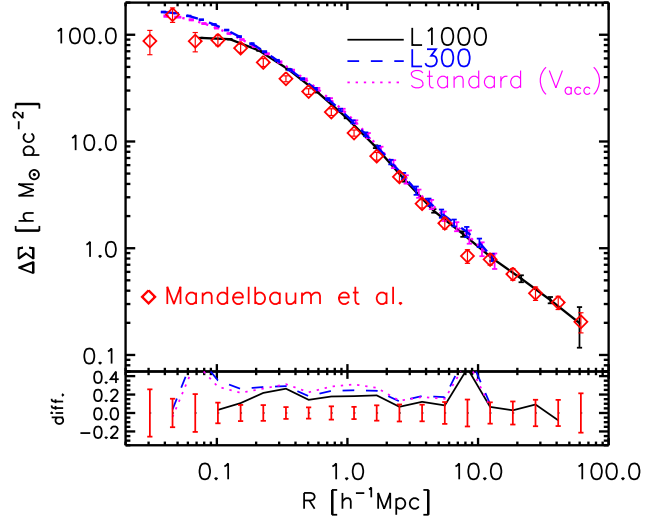


Figure 9. *Top Panel:* The average surface mass density profile around LRGs, which is an observable of the LRG-galaxy weak lensing. The solid and dashed curves are the results of our mock catalog, obtained by stacking N -body particles around all the LRG-host subhalos in the L1000 and L300 runs, respectively. The error bars are estimated using the measurements from 27 subsamples of LRG-host subhalos. The data with error bars show the SDSS measurements in Mandelbaum et al. (2012). As in Figures 3 and 8, we also show the result obtained from the standard abundance matching method (dotted curve). *Bottom panel:* The fractional differences of the model predictions compared to the measurement.

smaller than about $1 h^{-1}\text{Mpc}$ arises from the mass distribution within the same halo, while the signal at the larger scale arises from the mass distribution surrounding the host halos – the one- and two-halo terms, respectively (e.g. see Oguri & Takada 2011). The mock catalog well reproduces both the signals of different scales. The average halo mass inferred from the SDSS measurement is $\bar{M}_{\text{vir}} \simeq 4.1 \times 10^{13} h^{-1} M_{\odot}$ (Hikage et al. 2012a) (see also Table 1). Furthermore, the standard abundance matching method shows a similar-level agreement with the SDSS measurement, similarly to Figure 8.

Hikage et al. (2012a) also used the SDSS LRG catalog to study the weak lensing for the multiple-LRG systems. When making the lensing measurements, they used three different proxies for the halo center of each multiple-LRG system, the BLRG, FLRG and the arithmetic mean position of member LRGs (hereafter “Mean”). By comparing the lensing signals for the different centers, they constrained the average radial profiles of satellite BLRGs and FLRGs, finding about $400 h^{-1}\text{kpc}$ for a typical offset radius from the true center. Figure 10 shows that the mock catalog predictions are in remarkably good agreement with the SDSS measurements for the different centers. Since these lensing signals are from the exactly same catalog of the multiple-LRG systems, the differences between the different measurements should be due to the off-centering effects of the chosen centers. As nicely shown in Hikage et al. (2012a), the lensing signals for the BLRG and FLRG centers can be well explained by a mixture of the central and satellite BLRGs or FLRGs in the sample. The lensing signals for the FLRG center have smaller amplitudes due to the larger dilution effect because of a larger fraction of satellite (off-centered) FLRGs than in the BLRG centers. On the other hand, the Mean center does not have any galaxy (subhalo) at its position, and therefore the Mean center always has an off-centering effect from the true

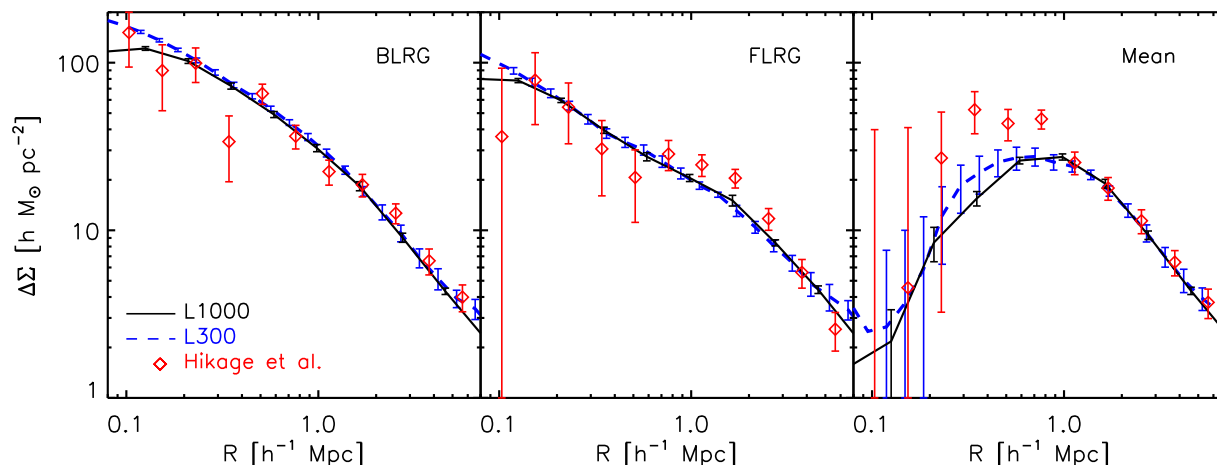


Figure 10. The average surface mass profiles for the multiple-LRG systems. The different panels show the results obtained by taking the different centers in each multiple-LRG halo; the brightest LRG (BLRG), the faintest LRG (FLRG) and the center-of-mass of different LRGs or the arithmetic mean positions of member LRGs (Mean) in the left, middle and right panels, respectively. The data with error bars show the SDSS measurements for the multiple-LRG systems in Hikage et al. (2012a).

center in each LRG system. This causes decreasing powers of the lensing signal at the smaller radii than the typical off-center radius. The lensing signals at some radii for the FLRG and Mean centers show some discrepancy from the mock catalog, but we do not think that the disagreement is significant. The average masses inferred from the SDSS measurement and the mock catalog for the multiple-LRG halos agree within about 30%; $\bar{M}_{\text{vir}} \simeq 1.46$ or $1.52 \times 10^{14} h^{-1} M_{\odot}$, respectively (also see Table 1).

As can be shown in Figures 8, 9 and 10, our mock catalog of LRGs well reproduces both the SDSS measurements for the auto-correlation function of LRGs and the LRG-galaxy weak lensing simultaneously. As recently discussed in Neistein & Khochfar (2012) (also see Neistein et al. 2011), the abundance matching method has a difficulty to reproduce these measurements with the same model, although they considered the spectroscopic sample of SDSS galaxies, rather than focused on LRGs. Thus the agreements of our mock catalog show a capability of our method to predict different statistical quantities of LRGs by self-consistently modeling, rather than assuming, the fractions of satellite LRGs among different halos and the radial distribution of satellite LRGs in the parent halos (also see Masaki et al. 2013, for a recent development on the extended abundance matching method based on the similar motivation).

3.4 Redshift-space power spectrum of LRGs

Another observable we consider is the redshift-space power spectrum of LRGs. The FoG effect due to internal motion of galaxies is one of systematic errors to complicate the cosmological interpretation of the measured power spectrum. The FoG effect involves complicated physics inherent in the evolution and assembly processes of galaxies, so is very difficult to accurately model from the first principles. One way to reduce the FoG contamination is to remove satellite galaxies from the region of each multiple-LRG system, and to keep only one galaxy (LRG in our case), ideally the central galaxy, because the central galaxy is supposed to be at rest with respect to the parent halo center and does not suffer from the FoG effect. For example, Reid et al. (2010) developed a useful method for this purpose; first, reconstruct the distribution of halos

from the measured distribution of LRGs by identifying multiple-LRG systems based on the CiC and FoF group finder method, and then keep only one LRG for each multiple-LRG system. However, the chosen LRG is not necessarily the central galaxy (more exactly, they used, as the halo center proxy, the arithmetic mean of member LRGs or the center-of-mass of different CiC groups without any luminosity or mass weighting), so there may generally remain a residual FoG contamination in the measured LRG power spectrum as pointed out in Hikage et al. (2012a).

In the left panel of Figure 11, we study the FoG effect on the redshift-space power spectrum, caused by the off-centering effect of LRGs in our mock catalog. Following the method in Reid et al. (2010) and Hikage et al. (2012a), we study the redshift-space power spectrum for LRG-host halos, instead of the power spectrum for LRGs. To compute the power spectrum of halos, we need to specify the halo center in each LRG-host halo. For single-LRG systems, we use the LRG position as the halo center proxy. For multiple-LRG systems, we employ different proxies of halo center for each system as done in Figure 10 for the LRG-galaxy lensing; BLRG, FLRG or the arithmetic mean (Mean), where the Mean center is computed in redshift space taking into account redshift space distortion due to peculiar velocities of LRG-subhalos. The figure shows the angle-averaged redshift-space power spectra for the different centers, relative to the power spectrum for the mass center of each LRG-host halo (the mass center of N -body particles of the host halo). Note that, for the power spectrum measurement, we used the exactly same catalog of LRG-host halos, and the different power spectra differ in the chosen halo center of each multiple-LRG system. Hence, the difference between the different spectra should be from the off-centering effects of the chosen centers in the multiple-LRG systems. Interestingly, the spectra for BLRG, FLRG and Mean centers all show smaller amplitudes with increasing wavenumber, as expected in the FoG effect. To be more precise, the power spectrum of FLRG center shows the strongest FoG effect, because a larger fraction of FLRGs are satellite galaxies than BLRGs (see Table 1). These results can be compared with Figure 2 in Hikage et al. (2012a). It can be found that the mock catalog qualitatively reproduces the SDSS measurements: the spectra

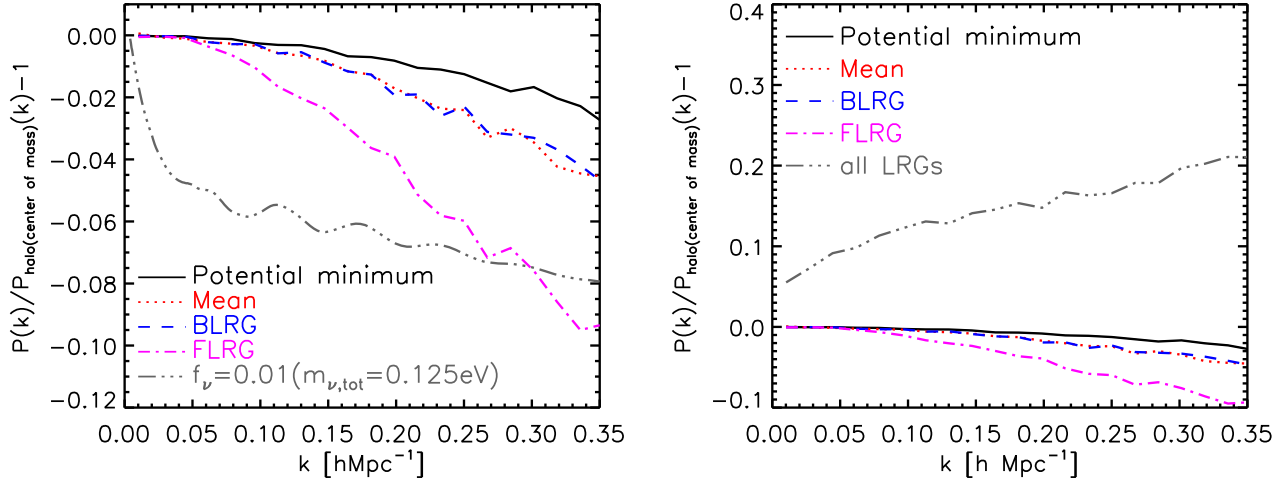


Figure 11. The angle-averaged redshift-space power spectra for the LRG-host halos at $z = 0.3$, computed from the L1000 run. The different curves show the fractional differences of the power spectra using different proxies of each LRG-host halo position in the power spectrum estimation, relative to the power spectrum for the mass center as the halo position. *Left panel:* The dotted, dashed and dot-dashed curves are the results when using different halo center proxies for each multiple-LRG system; the arithmetic mean position of the member LRGs in redshift space (Mean), BLRG or FLRG as in Figure 10. Note that we use the LRG position as the halo center for each single-LRG system. Thus the differences between the different spectra arise only from the different positions of multiple-LRG systems in redshift space, to be compared with Hikage et al. (2012a). The different power spectra show decreasing amplitudes with increasing wavenumber, which is caused by the nonlinear redshift-space distortion, the so-called Finger-of-God effect, due to the internal motions of the chosen halo centers in LRG-host halos. For comparison, we also show the power spectrum measured using the potential minimum of each LRG-host halo, where the potential minimum is the mass density peak of the smooth component of the halo that is likely to host the central galaxy. For comparison, the three dots-dashed curve shows the effect on the real-space matter power spectrum caused by massive neutrinos assuming the total neutrino mass $m_{\nu,\text{tot}} = 0.125 \text{ eV}$. *Right panel:* Similar to the left panel, but the power spectrum using all the LRGs is added (the three dots-dashed curve). The power spectrum includes contributions from multiple LRGs in the same halo. The shot noise contamination due to the different number densities of the LRG-host halos and the LRG-host subhalos is properly subtracted to have a fair comparison.

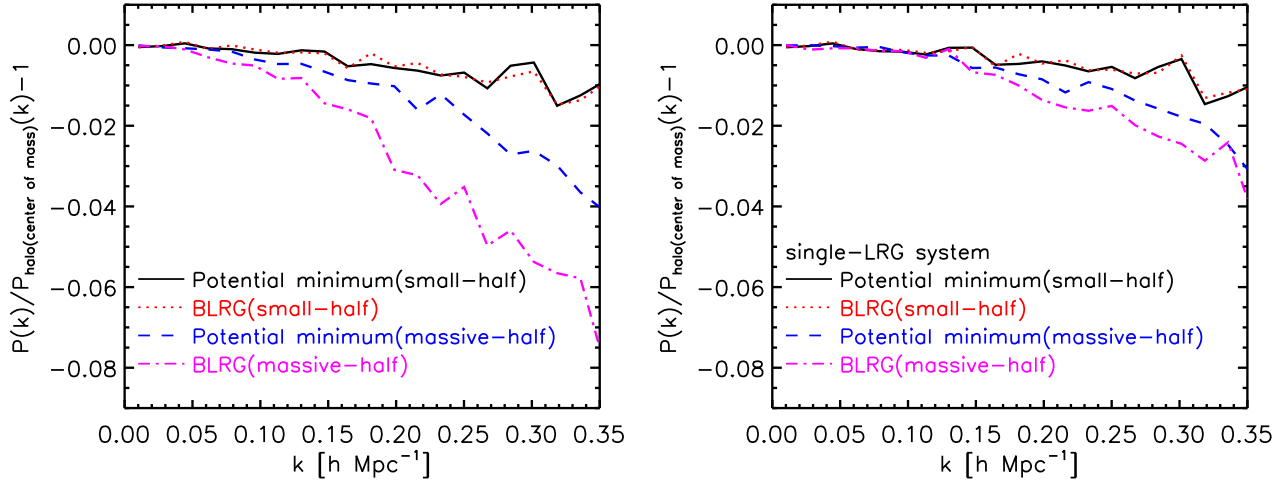


Figure 12. Similarly to the previous figure, but for the halved samples of LRG-host halos. *Left panel:* The LRG-halos are divided into two halved samples by the halo masses; one sub-sample is defined by halos which have masses smaller than the median mass (“small-half”), while the other is by halos with masses larger than the median (“massive-half”). The massive halo sub-sample shows a stronger FoG effect. *Right panel:* Similar plot, but using only the single-LRG halos.

of BLRG and Mean centers are similar, and the spectrum for FLRG shows the stronger FoG suppression.

Figure 11 also shows the power spectrum using the potential minimum as the center of each halo. We define the potential minimum as the mass density peak of smooth component: the central

subhalo position, in each LRG-host halo. In this part of the analysis, the power spectrum is measured by using the position of a central galaxy in each host halo. Again note that BLRG is not necessarily a central subhalo (galaxy) as shown in Figure 5. The power spectrum for the potential minimum has a smaller amplitude than that of the

mass center of host halo, implying that the potential minimum is moving around the mass center in each halo. Comparing the spectra for the potential minimum and the BLRG center shows that the BLRG spectrum has a smaller amplitude than the spectra for the potential minimum or the mass center by a few % in the fractional amplitude up to $k \simeq 0.3 h \text{ Mpc}^{-1}$. The few %-level FoG contamination would be okay for a current accuracy of the power spectrum measurement, but will need to be carefully taken into account for a higher-precision measurement of upcoming redshift surveys. For comparison, the three dots-dashed curve shows the effect on the real-space matter power spectrum caused by massive neutrinos, where we assumed $m_{\nu, \text{tot}} \simeq 0.1 \text{ eV}$ for the total mass of neutrinos, close to the lower limit on the neutrino mass for the inverted mass hierarchy. For the normal mass hierarchy, the lower limit on the total mass is about 0.05 eV, and the amount of the suppression is about half of the result of 0.1 eV in Figure 11. The lowest curve in the figure shows the difference of the real-space matter power spectrum when taking account of massive neutrinos relative to the spectrum for the mass-less neutrino cosmology.

In the right panel of Figure 11, we also show the redshift-space power spectrum derived by using all the LRGs in the catalog. Note that we properly subtracted the shot noise contamination from the measured power spectra by using the number densities of LRGs or LRG-host halos. In this case, the power spectrum ratio shows greater amplitudes with increasing wavenumber rather than the FoG suppression. That is, the LRG power spectrum shows a greater clustering power or greater bias than in the LRG-host halo spectrum. The scales shown here, the scales greater than a few tens Mpc, are much larger than a virial radius of most massive host-halos and the 1-halo term arising from clustering between two LRGs in the same host-halo should not be significant at these scales. Hence, the greater amplitudes in the LRG power spectrum would be due to a more weight on more massive halos, because satellite LRGs preferentially reside in more massive halos that have larger biases. Since the effect of different linear bias should cause only a scale-independent change in the power spectrum ratio, the change in the LRG power spectrum should be from a stronger non-linear bias of such massive halos, even though the FoG suppression should be more significant for such halos. In fact, a combination of the perturbation theory of structure formation and halo bias model seems to reproduce such a non-trivial behavior in the power spectrum amplitudes (Nishizawa et al. 2012). The results in the figure imply that including satellite LRGs in the power spectrum analysis complicates the interpretation of the measured power spectrum, thereby causing a bias in cosmological parameters. These subtle effects need to be well understood if we are going to use power spectrum measurements to place unbiased constraints on cosmological parameters such as the neutrino mass.

In Figure 12, we study how the residual FoG effect varies with masses of LRG-host halos. To study this, we divide the LRG halos into two sub-samples by masses of the LRG-halos smaller and larger than the median, and measured the fractional power spectra for each sub-sample relative to the halo sample. As expected, the FoG effect is larger for the sub-sample containing more massive halos, because of the higher fraction of satellite BLRGs as well as the larger velocity dispersion (larger halo mass). The right panel shows the similar results, but obtained only by using the single-LRG halos. First of all, the single LRG systems have a smaller FoG effect, because of the smaller fraction of satellite BLRGs (Figure 5 and Table 1) as well as the smaller velocity dispersions for the lower-mass host-halos. Among the single-LRG halos, more massive halos have relatively a larger FoG contamination, but only by a few percent at

$k \lesssim 0.35 h \text{ Mpc}^{-1}$ in the amplitude. Thus, the use of single-LRG systems may allow a cleaner interpretation of the measured power spectrum, yielding a more robust, unbiased constraint on cosmological parameters.

4 DISCUSSION AND CONCLUSION

In this paper, we have developed a new abundance-matching based method to generate a mock catalog of the SDSS LRGs, using catalogs of halos and subhalos in N -body simulations. A brief summary of our method is as follows: (1) identify LRG-progenitor halos at $z = 2$ down to a certain mass threshold until the comoving number density of the halos become similar to that of the SDSS LRGs at $z = 0.3$ (2) trace the merging and assembly histories of the LRG “star particles”, the 30% innermost particles of each $z = 2$ -LRG-progenitor halo that are gravitationally, tightly-bounded particles, and (3) at $z = 0.3$, identify the subhalos and halos hosting the LRG “star” particles. If a subhalo at $z = 0.3$ contains more than 50% of the star particles of any progenitor halo, we assign the subhalo at $z = 0.3$ as an LRG-host subhalo. We should emphasize that our method does not employ *any* free fitting parameter to adjust in order for the model to match the measurements, once the mass threshold of the LRG-progenitor halos is determined to match the number density of SDSS LRGs. Thus, by assuming that a majority of stellar components of LRG is formed at $z = 2$, we can trace the assembly and merging histories of LRGs over a range of redshift, $z = [0.3, 2]$; for example, we can directly trace which LRGs become central or satellite galaxies in the LRG-host halos at $z = 0.3$. The novel aspect of our approach is that the abundance matching of halos to a particular type of galaxies (LRGs in this paper) is done by connecting the halos and subhalos at different redshifts ($z = 2$ and $z = 0.3$ in our case), while the standard method is done for the same or similar redshift to the redshift of target galaxies. In addition, central and satellite subhalos are populated with galaxies under a single criterion: if a subhalo at $z = 0.3$ is a descendant of the $z=2$ -halos, the subhalo is included. The standard abundance matching uses different quantities for central and satellite subhalos, e.g., the circular velocities at the galaxy redshift and at the accretion epoch, respectively.

Using the mock catalog, we have computed various statistical quantities: the halo occupation distribution, the projected correlation function of LRGs, the mean surface mass density profile around LRGs (which is an observable of the LRG-galaxy weak lensing), and the redshift-space power spectrum of LRGs. We showed that the mock catalog predictions are in a good agreement with the measurements from the SDSS LRG catalog (Figures 3, 8, 9, 10 and 11). Thus our method seems to capture an essential feature of LRG formation in terms of a hierarchical structure formation scenario of Λ CDM model.

In the SDSS sample, about 5% of the halos contain multiple LRGs. In our simulation, 8% of the halos contain multiple LRGs. This modest deviation may be due to our simplified assumptions. First, we assumed that LRG progenitors are formed at a single epoch, $z = 2$. This is too simplified assumption as LRG formation almost certainly took place over a range of redshifts. Including a broader period of formation of LRG-progenitor halos may improve the model prediction. Second, although LRGs are observationally selected by magnitude and color cuts, our definition of the LRG-progenitor halos at $z = 2$ is solely based on their masses. The agreements between our mock catalog and the SDSS measurements support that the matching based on the LRG-progenitor halo

masses seems fairly reasonable to mimic a population of LRGs. However, the model may be further refined by combining masses of the progenitor halos with other indicators when matching to LRGs. For instance, using the maximum circular velocity of each halo instead of its mass may improve the model accuracy. Another potential improvement would be to introduce some stochasticity into the relationship between halo mass and inclusion in the LRG sample. Variation in star formation histories should introduce scatter into the halo mass/galaxy luminosity relation. We have done a preliminary study where we introduce some scatter and find that this lowers the characteristic halo mass, which leads to smaller bias parameters, and obviates the disagreement between theory and observation for the projected correlation function or the lensing mass profile in Figures 8 and 9. Another simplifying assumption was our neglect of satellite subhalos in the parent halo at $z = 2$ in the abundance matching procedure. We naively expect that subhalos at $z = 2$ merge into central subhalos from $z = 2$ to $z = 0.3$ due to dynamical friction, so we used the simplest method as the first attempt. However, including the subhalos at $z = 2$ for the abundance matching may improve an accuracy of the mock catalog. We plan to explore these improvements in a future work.

Our mock catalog or more generally our abundance matching method offers several applications to measurements. First, Masjedi et al. (2008) showed that, by using the small-scale clustering signal and the pair counting statistics, LRGs are growing by about 1.7% per Gyr, on average from merger activity from $z = 1$ to $z \sim 0.3$. Our method directly traces how each LRG-progenitor halo acquires the mass from other LRG-progenitor halos by major or minor mergers from $z = 2$ to $z = 0.3$. Hence, we can compare the prediction of our mock catalog with the measurement for the mass growth rate of LRGs. By using the constraint, we may be able to further improve the mock catalog.

Second, our method can predict how the distribution of LRG-progenitor evolves in relative to dark matter distribution as a function of redshift. Thus, our mock catalog can be used to predict various cross-correlations of LRG positions with other tracers of large-scale structure. As one such example, in this paper, we have studied the LRG-galaxy weak lensing measured via cross-correlation of LRGs with shapes of background galaxies, and have shown a remarkably good agreement between our model and the SDSS measurements. Another cross-correlation that has been studied in the literature is a cross-correlation of LRGs with a map of cosmic microwave background (CMB) anisotropies, which probes the stacked Sunyaev-Zel'dovich (SZ) effect (Hand et al. 2011; Sehgal et al. 2013) or the lensing effect on the CMB. Since every massive halos always host at least one LRG (100% of halos with $M_{\text{vir}} \geq 2 \times 10^{14} h^{-1} M_{\odot}$ in our mock catalog), the cross-correlation is a powerful cross-check of the SZ signals. Our mock catalog can predict how the stacked SZ signals change for different catalogs of LRGs such as an inclusion of satellite LRGs and multiple-LRG systems, which may be able to resolve some tension between the observed LRG-CMB cross-correlation signal and the theoretical expectation (Sehgal et al. 2013).

Third is an application of our method to LRGs or massive red galaxies at higher redshift than $z = 0.3$. The SDSS-III BOSS survey is now carrying out an even more massive redshift survey of SDSS imaging galaxies. The magnitude and color cuts used for the BOSS survey are designed to efficiently select galaxies at $0.4 < z < 0.7$, and are different from the SDSS-I/II LRG selection. The BOSS galaxies are called the ‘‘constant mass’’ (CMASS) galaxies. The majority of CMASS galaxies are early-type galaxies, but are not exactly the same population as LRGs. In addition, the

comoving number density of CMASS galaxies is higher than that of LRGs by a factor of 3. Hence, it would be interesting to apply the method developed in this paper to the CMASS galaxies. Figure 1 shows an interesting indication of our mock catalog: more LRG-progenitor halos survive in the $z = 0.5$ output than at $z = 0.3$, because the halos do not have enough time to experience merging due to the shorter time duration from $z = 2$ to $z = 0.5$ than to $z = 0.3$. Hence, our mock catalog naturally predicts a higher number density of LRG-progenitor halos at higher redshift than at $z = 0.3$, and may be able to match some of the BOSS galaxies without any fine tuning. Since the BOSS survey will provide us with a higher-precision clustering measurement and therefore has the potential to achieve tighter cosmological constraints, it is critically important to use an accurate mock catalog of the CMASS galaxies in order to remove or calibrate various systematic errors inherent in an unknown relation between the CMASS galaxies and dark matter. We hope that our method is useful for this purpose and can be used to attain the full potential of the BOSS survey or more generally upcoming redshift surveys for precision cosmology. This is our future study and will be presented elsewhere.

ACKNOWLEDGMENTS

We thank Kevin Bundy, Surhud More and David Wake for useful discussion and valuable comments. We also thank Rachel Mandelbaum, Zheng Zheng and Idit Zehavi for kindly giving us their SDSS measurement results. We appreciate Takahiro Nishimichi for kindly providing us with the second-order Lagrangian perturbation theory code. We also thank Naoki Yoshida for valuable advices for numerical techniques. We are grateful to the anonymous referee for helpful comments. SM acknowledges support from a Japan Society for Promotion of Science (JSPS) fellowship (No. 23-6573). This work was supported by JSPS Grant-in-Aid for Scientific Research Numbers 22340056 (NS), 23340061 (MT), 24740160 (CH) and NASA grant ATP11-0034 and ATP11-0090 (DS). MT greatly thanks Department of Astrophysical Sciences, Princeton University and members there for its warm hospitality during his visit, where this work was done. The authors acknowledge Kobayashi-Maskawa Institute for the Origin of Particles and the Universe, Nagoya University for providing computing resources useful in conducting the research reported in this paper. This research was in part supported by the Grant-in-Aid for Nagoya University Global COE Program, ‘‘Quest for Fundamental Principles in the Universe: from Particles to the Solar System and the Cosmos’’, from the Ministry of Education, Culture, Sports, Science and Technology (MEXT) of Japan, by JSPS Core-to-Core Program ‘‘International Research Network for Dark Energy’’, by Grant-in-Aid for Scientific Research from the JSPS Promotion of Science, by Grant-in-Aid for Scientific Research on Priority Areas No. 467 ‘‘Probing the Dark Energy through an Extremely Wide & Deep Survey with Subaru Telescope’’, by World Premier International Research Center Initiative (WPI Initiative), MEXT, Japan, by the FIRST program ‘‘Subaru Measurements of Images and Redshifts (SuMIRE)’’, CSTP, Japan, and by the exchange program between JSPS and DFG.

REFERENCES

- Anderson L. et al., 2012, MNRAS, 427, 3435
- Berlind A. A., Weinberg D. H., 2002, ApJ, 575, 587
- Blake C., et al., 2011, MNRAS, 415, 2876

- Bryan G. L., Norman M. L., 1998, *ApJ*, 495, 80
 Carson D. P., Nichol R. C., 2010, *MNRAS*, 408, 213
 Cole S., et al., 2005, *ApJ*, 362, 505
 Conroy C., Shapley A. E., Tinker J. L., Santos M. R., Lemson G., 2008, *ApJ*, 679, 1192
 Conroy C., Wechsler R. H., Kravtsov A. V., 2006, *ApJ*, 647, 201
 Crocce M., Pueblas S., Scoccimarro R., 2006, *MNRAS*, 373, 369
 Davis M., Efstathiou G., Frenk C. S., White S. D. M., 1985, *ApJ*, 292, 371
 Davis M., Huchra J., 1982, *ApJ*, 254, 437
 Dawson K. S. et al., 2013, *AJ*, 145, 10
 de Lapparent V., Geller M. J., Huchra J. P., 1986, *ApJ*, 302, L1
 Eisenstein D. J. et al., 2001, *AJ*, 122, 2267
 Eisenstein D. J., Hu W., Tegmark M., 1999, *ApJ*, 518, 2
 Eisenstein D. J., et al., 2005, *ApJ*, 633, 560
 Ellis R. et al., 2012, *ArXiv e-prints*, 1206.0737
 Gao L., Navarro J. F., Frenk C. S., Jenkins A., Springel V., White S. D. M., 2012, *MNRAS*, 425, 2169
 Hand N. et al., 2011, *ApJ*, 736, 39
 Hikage C., Mandelbaum R., Takada M., Spergel D. N., 2012a, *ArXiv e-prints*, 1211.1009
 Hikage C., Takada M., Spergel D. N., 2012b, *MNRAS*, 419, 3457
 Hopkins A. M., Beacom J. F., 2006, *ApJ*, 651, 142
 Kauffmann G., 1996, *MNRAS*, 281, 487
 Kirshner R. P., Oemler, Jr. A., Schechter P. L., Shectman S. A., 1987, *ApJ*, 314, 493
 Komatsu E. et al., 2011, *ApJS*, 192, 18
 Kravtsov A. V., Berlind A. A., Wechsler R. H., Klypin A. A., Gottlöber S., Allgood B., Primack J. R., 2004, *ApJ*, 609, 35
 Lewis A., Challinor A., Lasenby A., 2000, *ApJ*, 538, 473
 Mandelbaum R., Seljak U., Cool R. J., Blanton M., Hirata C. M., Brinkmann J., 2006, *MNRAS*, 372, 758
 Mandelbaum R., Slosar A., Baldauf T., Seljak U., Hirata C. M., Nakajima R., Reyes R., Smith R. E., 2012, *ArXiv e-prints*, 1207.1120
 Masaki S., Lin Y.-T., Yoshida N., 2013, *ArXiv e-prints*, 1301.1217
 Masjedi M., Hogg D. W., Blanton M. R., 2008, *ApJ*, 679, 260
 Masjedi M. et al., 2006, *ApJ*, 644, 54
 Neistein E., Khochfar S., 2012, *ArXiv e-prints*, 1209.0463
 Neistein E., Weinmann S. M., Li C., Boylan-Kolchin M., 2011, *MNRAS*, 414, 1405
 Nishimichi T. et al., 2009, *PASJ*, 61, 321
 Nishizawa A. J., Takada M., Nishimichi T., 2012, *arXiv:1212.4025*
 Nuza S. E. et al., 2012, *ArXiv e-prints*, 1202.6057
 Oguri M., Takada M., 2011, *Phys. Rev. D*, 83, 023008
 Peacock J. A., Smith R. E., 2000, *MNRAS*, 318, 1144
 Peacock J. A., et al., 2001, *Nature*, 410, 169
 Percival W. J., et al., 2007, *ApJ*, 657, 51
 Reddick R. M., Wechsler R. H., Tinker J. L., Behroozi P. S., 2012, *ArXiv e-prints*, 1207.2160
 Reid B. A., Spergel D. N., 2009, *ApJ*, 698, 143
 Reid B. A., et al., 2010, *ApJ*, 404, 60
 Saito S., Takada M., Taruya A., 2011, *Phys. Rev. D*, 83, 043529
 Schlegel D. J., et al., 2009, *ArXiv e-prints*, 0904.0468
 Scoccimarro R., Sheth R. K., Hui L., Jain B., 2001, *ApJ*, 546, 20
 Sehgal N. et al., 2013, *ApJ*, 767, 38
 Seljak U., 2000, *MNRAS*, 318, 203
 Seo H.-J., Eisenstein D. J., Zehavi I., 2008, *ApJ*, 681, 998
 Springel V., 2005, *MNRAS*, 364, 1105
 Springel V., White S. D. M., Tormen G., Kauffmann G., 2001a, *MNRAS*, 328, 726
 Springel V., Yoshida N., White S. D. M., 2001b, *NewA*, 6, 79
 Tegmark M., et al., 2004, *ApJ*, 606, 702
 Tojeiro R. et al., 2012, *MNRAS*, 424, 136
 Trujillo-Gomez S., Klypin A., Primack J., Romanowsky A. J., 2011, *ApJ*, 742, 16
 Wake D. A. et al., 2006, *MNRAS*, 372, 537
 Wake D. A. et al., 2008, *MNRAS*, 387, 1045
 Wang Y., Spergel D. N., Strauss M. A., 1999, *ApJ*, 510, 20
 White M. et al., 2011, *ApJ*, 728, 126
 York D. G. et al., 2000, *AJ*, 120, 1579
 Zehavi I. et al., 2005, *ApJ*, 621, 22
 Zheng Z., Coil A. L., Zehavi I., 2007, *ApJ*, 667, 760

APPENDIX A: VARIANTS OF OUR ABUNDANCE MATCHING METHOD

Although we have developed the simplest abundance matching method by connecting halos at $z = 2$ to subhalos at $z = 0.3$, the method rests on some simplified settings or assumptions that are not obvious: (1) the formation redshift of LRG-progenitor halos is set to a single epoch of $z = 2$, (2) we defined the “LRG-star-particles” by the innermost 30% particles of each $z = 2$ -progenitor halo, and (3) the “matching” fraction of the star particles to each subhalo at $z = 0.3$ is set to more than 50% (if a subhalo at $z = 0.3$ contains more than 50% of the star particles of any $z = 2$ -progenitor halo, the subhalo is called as the LRG-host subhalo). In summary, for our fiducial method, we have used

$$z_{\text{form}} = 2, f_{\text{star}} = 0.3, \text{ and } f_{\text{match}} = 0.5, \quad (\text{A1})$$

as described in detail in Section 2. In this Appendix, we study how the results are changed if varying each of these parameters to other values. In doing this, we use the L300 run because it has a higher resolution than L1000 run and allows us to better resolve less massive halos or sub-halos from the $z = 2$ or $z = 0.3$ simulation outputs.

A1 LRG-progenitor halo formation redshift: z_{form}

Throughout this paper, we employed $z_{\text{form}} = 2$ for the formation redshift of LRG-progenitor halos, as the first attempt, motivated by the fact that LRGs typically have old ages $\gtrsim 5$ Gyr. Figure A1 shows how the mock catalog of LRGs is changed if varying the formation redshift to $z_{\text{form}} = 1$ or 3 from our fiducial choice $z_{\text{form}} = 2$. Here, to assess the difference, we show the projected correlation functions obtained from the mock catalogs. The figure shows that the formation redshift of $z_{\text{form}} = 1$ or 3 gives lower or higher amplitudes at small separations $\lesssim 1 h^{-1} \text{Mpc}$, which is in the one-halo term regime, than our fiducial case of $z_{\text{form}} = 2$. Nevertheless, the encouraging result is that the large-separation correlation function in the two-halo regime is not largely changed. These changes can be understood as follows. For the case of $z_{\text{form}} = 1$, the LRG-progenitor halos have a shorter duration since the formation and each halo has a smaller chance to experience subsequent mergers than in the case of $z_{\text{form}} = 2$, the progenitor in turn has a smaller chance to be included in multiple-LRG systems being a satellite subhalo at $z = 0.3$, which decreases clustering power in the one-halo regime. Thus Figure A1 implies that a choice of $z_{\text{form}} \gtrsim 2$ is reasonable.

The upper panel of Figure A2 shows how the change of z_{form} alters the HOD as in Figures 3. As we discussed above, the change

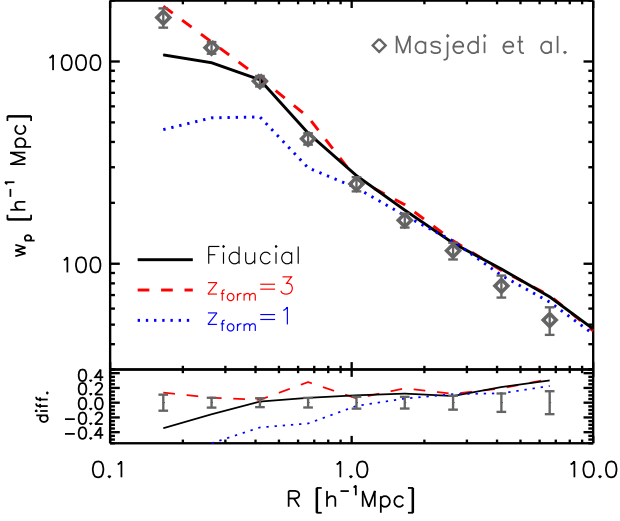


Figure A1. Shown is how the model prediction of the projected correlation function is changed if varying the model parameter in our abundance matching method, in comparison with the SDSS measurement as in Figure 8. This plot shows the correlation functions from the mock catalogs obtained by changing the formation redshift of LRG-progenitor halos from $z_{\text{form}} = 2$ (our fiducial choice) to $z_{\text{form}} = 1$ or 3. The different formation redshifts change the prediction mainly at the small scales, in the one-halo regime, because it changes a time duration for each progenitor halo to experience subsequent merging and assembly histories. For example, if changing to $z_{\text{form}} = 1$, the progenitor halos do not have enough time to experience merger, which decreases a population of satellite LRGs (subhalos) and in turn leads to the decreased clustering power at the small scales.

to $z_{\text{form}} = 3$ from $z_{\text{form}} = 2$ leads to a smoother HOD shape around the cutoff halo mass for the central LRG HOD extending down to less massive halos as well as to an increase of satellite LRGs. The choice of $z_{\text{form}} = 1$ leads to opposite effects. On the other hand, the lower panel shows that the projected mass profile of LRG-host halos is almost unchanged by the change of z_{form} . Thus an accuracy of the mock catalog can be improved, especially for predicting the small-scale clustering, by further introducing a variation of the formation epochs as additional parameter.

A2 The fraction of LRG-star particles in

$z = 2$ -LRG-progenitor halo: f_{star}

To trace the LRG-progenitor halos from $z = 2$ to $z = 0.3$, we defined the LRG-star particles in each $z = 2$ LRG-progenitor halo by the 30% innermost particles of the FoF member particles, $f_{\text{star}} = 0.3$, assuming that the stars are formed at the central region of each halo. However, the fraction 30% is an arbitrary choice.

Figure A3 shows how the projected correlation and the HOD are changed by varying to $f_{\text{star}} = 0.2$ or 0.4 from the fiducial choice of $f_{\text{star}} = 0.3$. Note that, when matching each $z = 2$ -progenitor halo to a subhalo at $z = 0.3$, we imposed the condition that a subhalo at $z = 0.3$ should have more than 50% of the star particles in each of the mock catalogs. Figure A3 shows that the change of f_{star} alters the correlation function at the small separation, in the one-halo regime. This is also found from the lower panel, which shows that the change alters the satellite HOD. If we use $f_{\text{star}} = 0.4$ from 0.3, it tends to include, in the star particles, more loosely-bounded member particles in each $z = 2$ -progenitor halo, the star particles tend to be stripped by tidal interaction or

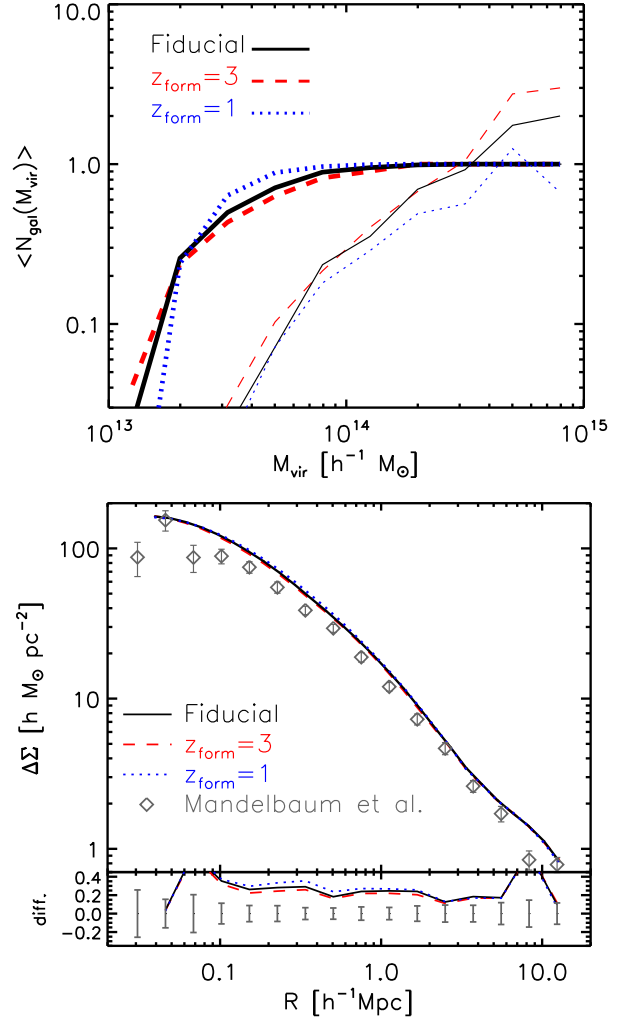


Figure A2. Similarly to the previous plot, but for the HOD (upper panel) and for the projected mass profile (lower).

merger with other halos, and then it is in turn difficult to satisfy the 50% matching condition to $z = 0.3$ subhalo. Thus this results in a smaller number of the survived satellite LRG-halos at $z = 0.3$, which causes to reduce the correlation amplitude at the small scales. The opposite is true for the case of $f_{\text{star}} = 0.2$, because it leads to a larger number of the survived satellite LRG-halos at $z = 0.3$ than in the case of $f_{\text{star}} = 0.3$. Nevertheless, the encouraging result is the correlation function at large scales in the two-halo regime is not sensitive to the variation of f_{star} . We have found that the projected mass profile is not changed as in the lower panel of Figure A2.

A3 The matching fraction between $z = 2$ -LRG-progenitor halos and $z = 0.3$ -subhalos: f_{match}

Finally, we study how the mock catalog is changed by varying the matching fraction to $f_{\text{match}} = 0.3$ or 0.7 from our fiducial choice $f_{\text{match}} = 0.5$. Figure A4 shows that the change of f_{match} alters the projected correlation function at small scales in the one-halo regime and the satellite HOD, similarly to Figures A1 and A3. Again, if increasing the matching fraction to $f_{\text{match}} = 0.7$ from 0.5, it leads

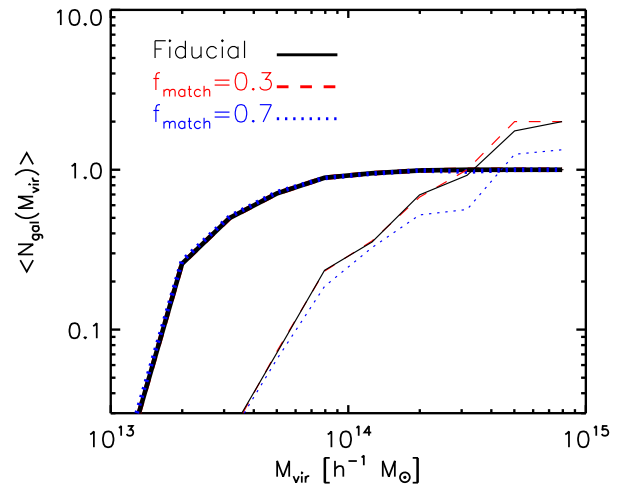
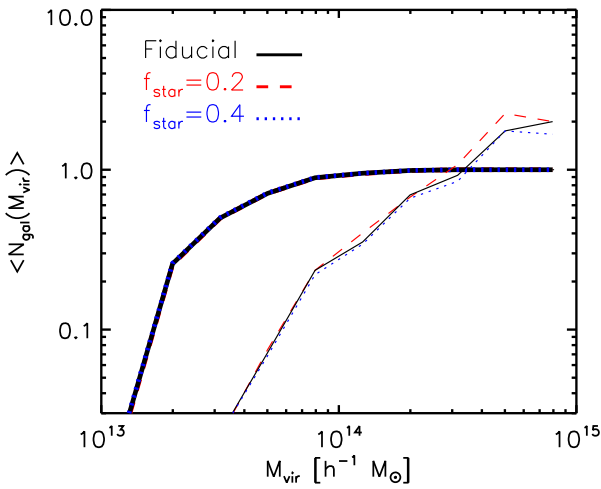
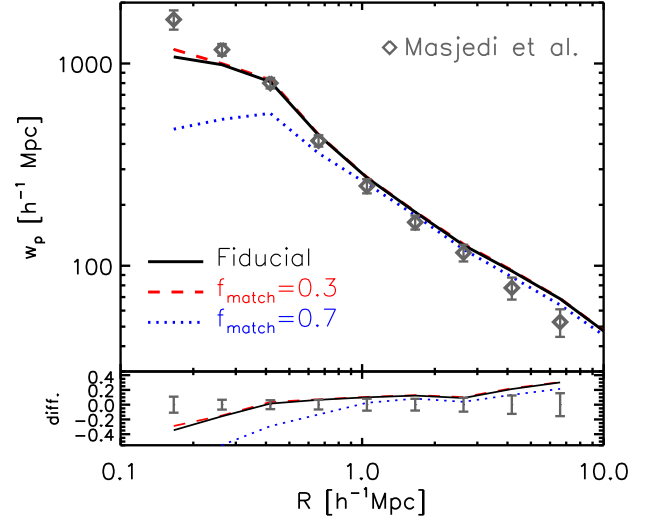
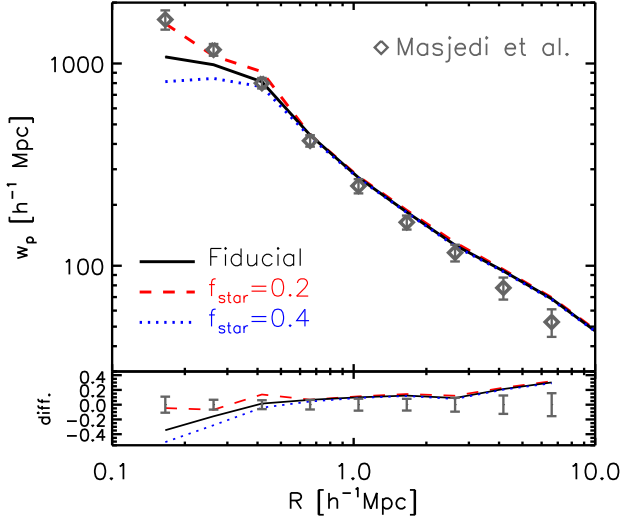


Figure A3. Similarly to the previous figure, but this plot shows the impact of the parameter f_{star} on the correlation function prediction (*upper panel*) and on the HOD (*lower*), where f_{star} is used to define “LRG-star” particles in each LRG-progenitor halo at $z = 2$ by the f_{star} -fraction of innermost member particles in the halo. Again, changing $f_{\text{star}} = 0.2$ or 0.4 from our fiducial choice $f_{\text{star}} = 0.3$ alters the model prediction at the small scales.

Figure A4. Similarly to the previous figure, but this plot show the impact of the matching fraction parameter f_{match} . In the case of $f_{\text{match}} = 0.5$ (our fiducial choice), a subhalo at $z = 0.3$ is called as LRG-host subhalo if the subhalo contains more than 50% of the star particles in an LRG-progenitor halo at $z = 2$. The different curves show the results for $f_{\text{match}} = 0.3$ or 0.7 , which differ from our fiducial model at the small scales.

to a less number of the matched satellite subhalos at $z = 0.3$ and in turn leads to a decreased power in the correlation function. On the other hand, the large-scale correlation is more robust to the change of f_{match} similarly to the previous figures. We have again found that the projected mass profile is not changed as in the lower panel of Figure A2.